UNIVERSITY OF CALIFORNIA, MERCED

Tribological Effects of Temperature and Surface Roughness on the Performance of Electric Motor Greases with Hybrid Bearing Materials

A Thesis submitted in partial satisfaction of the
requirements for the degree
Master of Science

in

Mechanical Engineering

by

Daniel Eduardo Sanchez Garrido

Committee in charge:

Ashlie Martini, Chair
Mehmet Z. Baykara
Roberto C. Andresen Eguiluz

2021

This Thesis of Daniel Eduardo Sanchez Garrido is approved, and it is acceptable in quality and form for publication on microfilm and electronically:

Ashlie Martini, Chair Date

Mehmet Z. Baykara Date

Roberto C. Andresen Eguiluz Date

University of California, Merced

2021

Para mis padres aquien les debo todo.

Gracias!

ABSTRACT

Electric Vehicles (EVs) are emerging as the future of transportation as the market moves towards electrification. However, materials and lubricants for EVs have not been optimized over decades of tribological research like it has been done for internal combustion engine vehicles (ICEVs). Although EVs are more efficient than ICEVs, energy losses and tribological challenges in electric motors (EMs) are still considerable, so characterization of EM-specific friction and wear behavior is important. Particularly, greased bearings in EMs are subject to a wide range of operational requirements and corresponding micro-environments. Consequently, greases must function effectively in these conditions. Here, the tribological performance of four market-available EM greases was characterized by measuring friction and wear of silicon nitride sliding on hardened 52100 steel. The EM greases evaluated had similar viscosity grade, but different combinations of polyurea or lithium thickener with mineral or synthetic base oil. Measurements were performed across a range of temperatures and surface roughness conditions to capture behavior across multiple lubrication regimes. Results enabled direct comparison of market-available products across different application-relevant metrics and the analysis methods developed can be used as a baseline for future studies of EM grease performance.

TABLE OF CONTENTS

LIST OF FIGURES

LIST OF TABLES

Chapter 1

Introduction

1.1 Background

In this section, fundamental engineering principles, theory, and concepts of tribology will be established. These will serve as a foundation and background for the study.

1.1.1 Tribology

The field of tribology contains interdisciplinary science and engineering aspects focusing on the study and application of the principles of friction, wear and lubrication. These principles are observed between interacting surfaces in relative motion. Tribology is a phenomenon present in everyday life but, for most, it goes unnoticed. However, when it comes to mechanical systems, tribology is of great economic, environmental and engineering importance.

The economic impact of friction and wear burdens industrialized countries so tribology cannot be ignored [3]. The cost of friction and wear comes in terms of energy efficiency and material waste [3]. At a global scale, for societal sectors, the cost of tribology-related losses is estimated at 2536 billion euros ($\approx$ 3089 billion

United States Dollars (USD)) annually; 73% from friction and 27% as a result of wear [4]. Estimates for the United States of America suggest that advancements in tribology could alleviate about 11% of the total energy loss in transportation, turbo machinery, power generation and industrial processes [3]. Energy savings for vehicles in the United States alone would amount to about $14.3 billion USD per year [3].

Energy savings can also translate to positive environmental impacts. Friction and wear generate about 8,120 $MtC0_2$ per year of emissions [4]. About 28% of a vehicles energy from fossil fuels is lost to friction in the engine/transmission [3, 4]; tribological advancements would mitigate energy loss which would reduce fossil fuel consumption and consequently reduce emissions/carbon footprint. Global implementation of new technologies capable of reducing energy losses could potentially save 1,460 $MtCO_2$ emissions which translates to 455 billion euros (≈554 billion USD) annually [4].

Engineering systems that are more energy efficient will heavily depend on advancements in tribology. Such advancements can be achieved via research. At a global scale, the implications of even the most minor of reductions in friction and energy consumption would be significant given the number of mechanical systems [6, 4]. Fundamentally, tribology comes down to managing friction and wear; when applicable, a lubricant can be implemented to help manage the contact between interacting surfaces.

1.1.2 Friction

Friction can be understood as the resistance to relative motion. Mathematically, the coefficient of friction can be expressed as:

$$\mu = \frac{F}{W} \tag{1.1}$$

Where μ is the coefficient of friction, F is the frictional force and W is the normal force [2]. Therefore, the coefficient of friction is the ratio of the frictional force and normal load; the magnitudes of F and W are proportional to each other [2, 1].

Friction can occur between interacting surfaces as well as in non-solid lubricants resulting from fluid shear. The coefficient of friction resulting from interacting surfaces can be classified as static friction (μ_s) or kinetic friction (μ_k). Static friction is the initial frictional force required to enable sliding conditions and kinetic friction is the frictional force required to sustain sliding conditions; note that $\mu_s > \mu_k$ [2]. Friction from fluid shear is known as viscous friction and is determined by the rheological properties of the lubricant; viscous friction is proportional to velocity [1]. Aside from empirical models with limited range, friction is difficult to predict because it depends on material properties, whether the contacts are lubricated or not, operating conditions and surface topography [1].

1.1.3 Wear

Wear is the loss of material from the interacting surfaces. The severity of wear will depend on the degree of lubrication failure [3], stresses, mechanical damage, thermal conditions, type of surface contact and chemical reactions [2]. Consequently, similar to friction, wear is a very complex process [1].

Generally, wear is measured as volume per unit distance so it can be expressed as a wear rate [1, 2]. A simple and popular model for sliding wear is known as the Archard wear equation:

$$Q = \frac{KW}{H} \tag{1.2}$$

here, Q is the volume worn per unit sliding distance, K is the wear coefficient, W is the normal load and H is hardness for the softer body [2]. Equation 1.2 is considered to provide useful wear information but should not be considered to be absolute [2, 1].

There are various types of wear mechanisms. These include but are not limited to fatigue wear, adhesive wear, abrasive wear, corrosive wear, erosive wear and cavitation wear. Fatigue wear results from repetitive stress on the contact under sliding or rolling [3, 2]. Adhesive wear occurs when the interacting surfaces cause plastic

shearing of asperity peaks causing them to adhere to the opposite body [1]. The term asperity refers to individual surface features (see section 1.1.4). Wear caused by a surface or particles that are harder than the contacting surface will remove or displace material from the softer surface causing abrasive wear [1, 3]. Corrosive wear is the result of chemical activity between interacting surfaces, worn material and a corroding medium that can lead to material displacement [3]. Erosive wear is caused by particles impacting a surface leading to material removal [3]. Cavitation occurs when a liquid ruptures due to stress causing voids [1], as these voids collapse on a surface they cause wear.

1.1.4 Surface Roughness

All solid surfaces have some type of topography in which asperities of different heights make up the surface. In fact, even the smoothest surface will have asperities larger than atomic dimensions [2]. To understand tribological behavior at the interface, it is important to first understand the topography, [1] since surface characteristics influence friction, wear and lubrication [3].

Surface topography or surface roughness can be studied and measured through different methods. These methods can include both contact or non-contact forms of surface examination. For a non-contact approach, instruments using electron or light microscopy as well as optical and capacitance methods can be employed [2]. Contact modes include stylus profilometry or scanning probe microscopy to survey the surface [1, 2]. Atomic force microscopy (AFM) is possibly the highest resolution technique but less sensitive approaches are enough to study most engineering surfaces [2].

As discussed above, measurements of a surface can be taken with different types of instruments. The line or area height data from such a measurement provides surface coordinates over an area which can be used to describe the surface roughness [2, 1]. This data includes roughness (short wavelength hills and valleys) and waviness

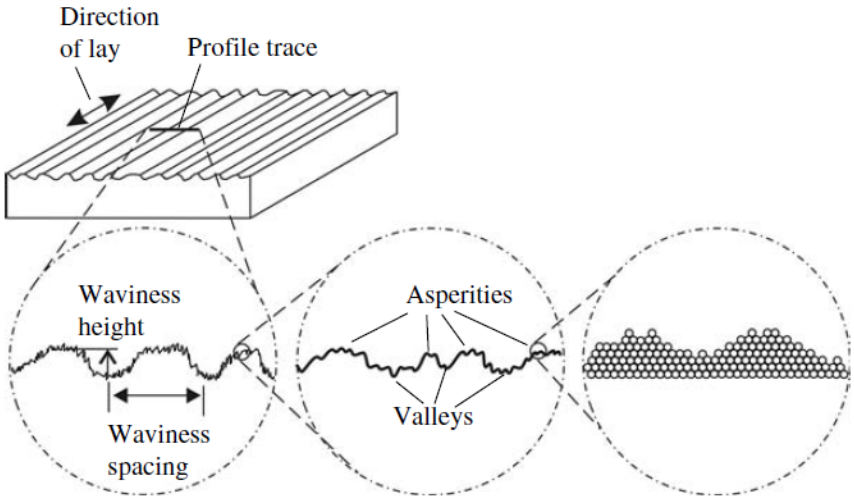

Figure 1.1: Sample with a certain surface topography **(top)**. **(Bottom)** Different levels of magnification reveal different levels of roughness down to atomic scale [1].

(surface features with larger spacing than roughness features and small variations of spacing and amplitude) [1]. Instrument sensitivity will determine resolution quality. Fig. 1.1 depicts the surface of a sample and, upon further and further magnification, nested levels of asperities and different roughness scales down to the atomic level are revealed [1].

Several quantitative measures can be derived from a data set that contains information about a surface topography [2]. The four most common quantitative measures or roughness parameters used are average roughness (Ra), root mean square roughness (Rq), skewness (Rsk) and kurtosis (Rku). Ra is the most popular parameter of the four and is defined as the mean deviation of the surface height from a mean line of the profile [2]; see Fig. 1.2.

$$Ra = \frac{1}{L}\int_0^L |z(x)|\,dx \tag{1.3}$$

or:

$$Ra = \frac{1}{N}\sum_{i=1}^{N}|z_i| \tag{1.4}$$

here z is the surface height from the mean height, L is the sampling length or for discrete points of N number of z heights to the ith point. Rq is the root mean square deviation of the profile from the mean height [2].

$$Rq = \sqrt{\frac{1}{L}\int_0^L (z(x))^2\,dx} \tag{1.5}$$

or:

$$Rq = \sqrt{\frac{1}{N}\sum_{i=1}^{N} z_i^2} \tag{1.6}$$

Ra and Rq are similar for most surfaces and $Rq = 1.25Ra$ for a Gaussian distribution of heights [2]. However, Ra and Rq are not enough to describe surface features. Therefore, to avoid losing important information about a surface topography, Rsk and Rku are necessary. Rsk provides a measure of surface asymmetry which describes the shapes of surface irregularities and their vertical extent [2]. Rsk is defined as:

$$Rsk = \frac{1}{Rq^3}\frac{1}{L}\int_0^L (z(x))^3\,dx \tag{1.7}$$

or:

$$Rsk = \frac{1}{Rq^3}\left[\frac{1}{N}\sum_{i=1}^{N} z_i^3\right] \tag{1.8}$$

Note that Rsk can be positive or negative and is dominated by heights furthest from the mean line, i.e. large peaks and relatively small valleys will lead to a positive skewness [2]. Lastly, kurtosis (Rku) indicates the sharpness of the peak of the distribution

curve [2]. *Rku* is defined as:

$$Rku = \frac{1}{Rq^4}\frac{1}{L}\int_0^L (z(x))^4\,dx \tag{1.9}$$

or:

$$Rku = \frac{1}{Rq^4}\left[\frac{1}{N}\sum_{i=1}^{N} z_i^4\right] \tag{1.10}$$

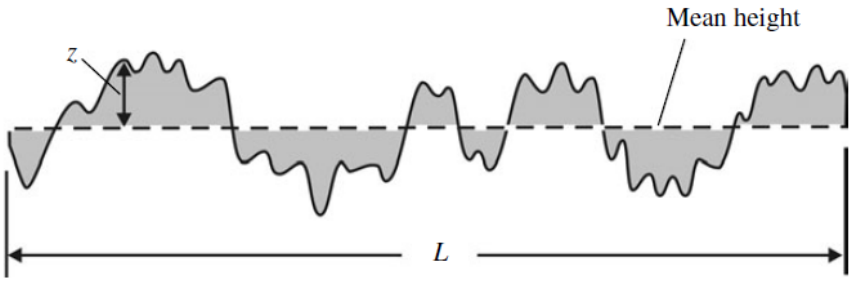

Figure 1.2: Sample surface profile of length L, height z and mean height (dashed line). [1].

1.1.5 Lubricants

Lubricants are used and designed to lubricate mechanical systems. Mainly, a lubricant works by forming a layer between interacting surfaces to reduce shear strength (shear stress required to initiate and maintain sliding) [1, 2]. The layer of lubrication can vary in thickness and is often referred to as film thickness. The film thickness of a lubricant determines friction and wear of an interface.

Various types of material can be used as a lubricant, including liquid, semi-solid, solid and gas. For example, liquid lubricants such as oils can originate from biological and non-biological hydrocarbon substances [3]. Generally, lubricating oils are composed of 75-95% base oil and 5-25% additives [3, 2]; see Fig. 1.3. Biological oils or mineral base oils are refined until desired properties for lubrication are achieved

[3]. Synthetic base oils are made artificially and are designed to replace and provide superior properties than mineral oils [3]. Lubricant additives are chemicals added to a formulation to change the lubricants properties, overall performance and prolong life [3, 2].

Function	Component	Concentration (wt%)
Base oil (mineral or synthetic)		75–95
Friction and wear	VI improver	0–6
	Antiwear additive	0.5–2
	Friction modifier	0–2
	Corrosion inhibitor	0–1
Contamination/cleanliness	Antioxidant	0–1
	Dispersant	1–10
	Detergent	2–8
Maintain fluid properties	Pour-point depressant	0–0.5
	Anti-foam additive	0–0.001

Figure 1.3: Typical lubricant base oil and additive composition along with additive function/component breakdown [2].

Semi-solid lubricants, i.e. grease, are similar to lubricating oils. The main difference between the two is that greases contain a thickening agent as part of their formulation [3, 7]. Thus, grease formulations consist of 3-30% thickener (disperse phase), and the rest is composed of base oil and additives [7]. The thickener structure determines grease consistency and the intermolecular forces between thickener molecules will determine base oil retention and bleeding properties [7]. Therefore, different thickeners will have different structure and thus, different properties and lubricating performance capability [7].

Solid lubricants are typically used as surface coatings. These type of lubricants provide superior cleanliness, operate at extreme temperatures, under vacuum, and/or radioactive environments [3]. For example, solid lubricants such as graphite and molybdenum disulfide can be used to layer contacting surfaces [3, 2]. Solid lubricants can also take the form of a solid substance to be used at high wear locations or parts

in machinery [3].

Gaseous lubricants typically have lower viscosity when compared to liquid or solid lubricants [8]. Air is a very common type of gas lubricant because it is widely available, does not degrade and poses minimal risks to the environment [1]. Gas lubricants typically lubricate certain type of bearings as well as some high speed applications [3]. A gas lubricant can offer non-toxic lubrication, great cleanliness, chemical stability over wider temperatures along with eliminating fire risks related to lubricants containing hydrocarbons [3]. Note that each type of lubricant will have advantages and disadvantages, depending on operating environment and conditions.

1.1.5.1 Greases Versus Lubricating Oils

Oil and grease lubrication have been employed since ancient times to reduce both friction and wear [1]. However, each of these types of lubricants have optimal operating conditions and environments in which they will perform more efficiently.

The choice of oil vs. grease depends on operating conditions. For example, in bearing applications that experience frictional heat, oil lubrication has better bearing cooling capabilities than grease [7, 2]. Superior cooling capabilities translate to healthier levels of viscosity and film thickness [7]. Additionally, because of their cooling and replenishment activity, oils are less impacted by aging [7]. Greases on the other hand, are more susceptible than oils to aging from oxidation resulting from high temperatures, mechanical work and contaminants [7].

However, in some cases, using grease for lubrication purposes has several advantages. For instance, grease is less likely than oil to be displaced from bearing surfaces or drain under gravity, this is because of its semi-solid consistency [7, 2]. Also, unlike oil, grease can provide a good seal against external contaminants [2] and promote bearing life [7]. Grease lubrication has also been associated with lower friction levels than those achieved with oil [7] but in certain cases risk higher friction due to viscous forces [2].

Oil selection is mainly dependent on viscosity, lubricity and additives [7]. Note that lubricity refers to the ability to reduce friction. On the other hand, grease selection will require additional considerations which adds complexity to the selection process. While the aspects considered for oil selection will also be important for selection of grease, grease selection will be dominated by thickener properties [7].

1.1.5.2 Viscosity

One of the most important properties that defines a lubricant's capabilities is viscosity. Viscosity is the resistance of a lubricant to shear [2, 1]. Viscosity is measured as dynamic or kinematic. Dynamic viscosity (η) is most relevant for calculations and is the ratio of shear stress and shear strain rate [1].

$$Dynamic\ Viscosity\ (\eta) = \frac{Shear\ stress}{Shear\ rate} \tag{1.11}$$

η has units of ($\frac{N \cdot s}{m^2}$) or can also be given as centipoise (cP); 100 cP = 1 Poise ($Pa \cdot s$). Kinematic viscosity on the other hand, has the following relationship [1]:

$$Kinematic\ Viscosity\ (v) = \frac{Dynamic\ viscosity}{Density} \tag{1.12}$$

kinematic viscosity has units of ($\frac{cm^2}{s}$) also known as a stokes (St). However, the most common unit for kinematic viscosity is centistokes (cSt) [1]; 1 St = 100 cSt ($\frac{mm^2}{s}$).

Viscosity is temperature dependent. With increasing temperature the viscosity of lubricants fall quickly [2, 1]. One method to describe viscosity behavior is by using lubricant industry grades such as International Standards Organization viscosity grades (ISO VG). ISO VG is determined using the ISO 3448 standard and calculated using known 40°C and 100°C kinematic viscosity values [2]. Viscosity behavior with temperature can also be described using the MacCoull-Walter equation [2]:

$$log_{10}\ log_{10}\ (viscosity\ in\ cSt + 0.7) = A - B\ log_{10}\ T \tag{1.13}$$

here T is temperature in units of kelvin and A & B are constants for a given fluid [2]. Equation 1.13 enables viscosity to be approximated for any temperature as long as two reference values are known (usually at 40 and 100°C).

Changes in viscosity will affect lubrication film thickness. Film thickness can have positive or adverse effects on friction and wear behavior. Consequently, lubricant viscosity can also determine the lubrication regime in which a system will operate.

1.1.6 Lubrication Regimes

Lubricants help separate surfaces to reduce friction and wear. The extent of a lubricants functionality to separate interacting surfaces will vary. In some systems, depending on the tribological conditions, a lubricant will not be fully capable of separating surfaces at the interface and thus allowing some asperity contact. Therefore, depending on the degree of lubrication at the interface, different lubrication regimes will be established.

There are three main lubrication regimes. These regimes are best depicted on the Stribeck curve and are known as full film lubrication, mixed lubrication and boundary lubrication as shown in Fig. 1.4. Essentially, the Stribeck curve illustrates how changes in sliding conditions will impact mechanisms of lubrication within a lubricated system [1]. The Stribeck curve is in terms of coefficient of friction versus lambda (λ) ratio (film thickness/ surface roughness) or alternatively the Hersey number (speed $\cdot$ viscosity/ pressure). Insets to Fig. 1.4 depict surface interaction and lubrication at the interface.

1.1.6.1 Full Film Lubrication

Full film lubrication occurs when a lubricating film is thick enough to fully separate two interacting surfaces. That is to say, film thickness is significantly greater than surface roughness [8]. In this regime, viscous forces within the lubricant provide

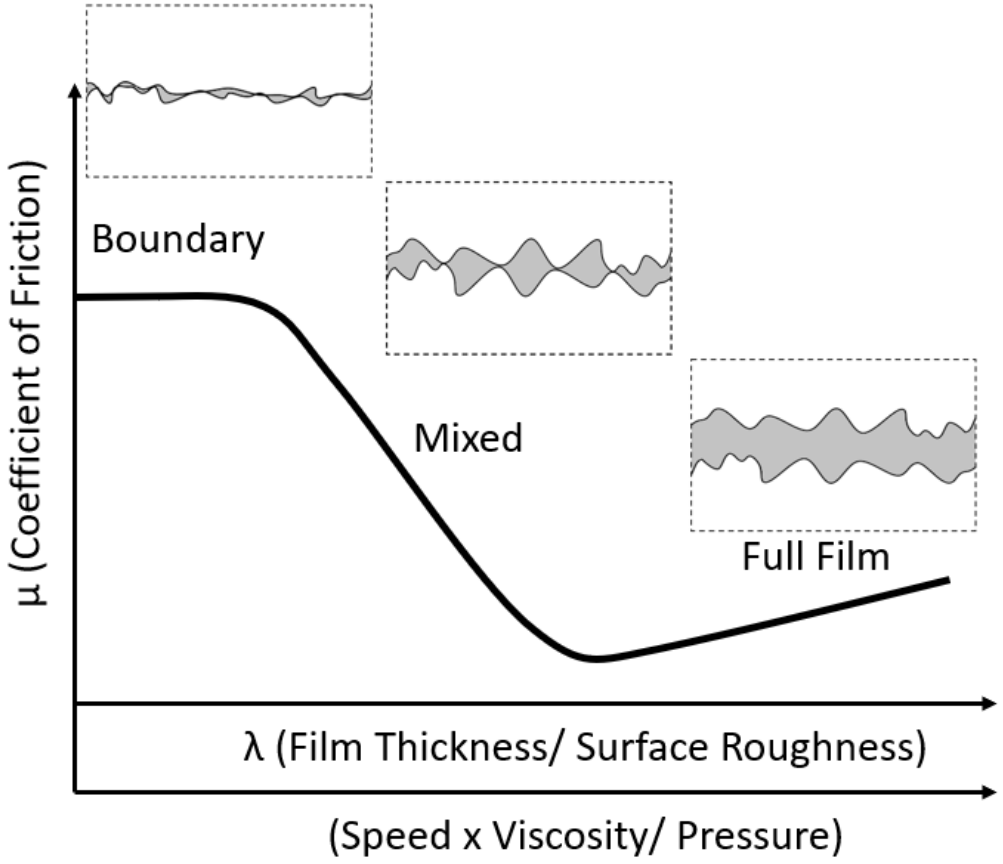

Figure 1.4: Typical Stribeck curve behavior depicting the main lubrication regimes in terms of coefficient of friction and λ ratio (film thickness/ surface roughness) or the Hersey number (speed $\cdot$ viscosity/ pressure). Representative interface interactions for each lubrication regime.

normal load support [2]. Typically, this regime is said to exist for λ ratios > 3 [8, 2]. It is also important to note that as λ increases in full film, friction also increases. The increase in friction here is due to internal resistance of the lubricant to motion [8] and is called viscous friction.

1.1.6.2 EHL and Film Thickness

ElastoHydrodynamic lubrication (EHL) is an important region of the full film regime. On the Stribeck curve, this region is located before the onset of mixed lubrication where friction and the lambda ratio are smallest in the full film regime. EHL is important because bearings typically operate in this region. In the EHL regime, both elastic deformation at the interface and changes in viscosity with pressure affect lubrication [3]. The hydrodynamic pressure distribution in EHL contact is given by Fig. 1.5a [3].

For lubricated bearing contacts in EHL, there are two possible forms of film thickness. One possibility is central film thickness (h_c) and the other is minimum film thickness (h_{min}); see Fig. 1.5a. These two film thickness possibilities come as a result of the elastic deformation of the contacting surfaces and the contact pressure. Central film thickness occurs at the inlet of the contact where h_c experiences a rise in viscosity as it enters the contact [3]. At the outlet of the contact, viscosity experiences an equally sharp decline to ambient viscosity and thus generates an area of minimum film thickness [3]. For h_{min}, the constriction generates a large peak in pressure and the magnitude of the peak will depend on the the lubricants pressure-viscosity characteristics [3]. The EHL contact area that contains both h_c and h_{min} gives a horseshoe like effect (Fig. 1.5b).

1.1.6.3 Mixed Lubrication

Mixed lubrication occurs when a lubricating film enables some separation between interacting surfaces but some asperity contact is also present. Here, film thickness and surface roughness can be on the same order of magnitude [8]. Therefore, in mixed lubrication the load can be supported by a combination of both film thickness and asperities [8]. In fact, as λ decreases in this regime, asperity contact at the interface is more likely to occur and thus, a larger portion of the load is supported

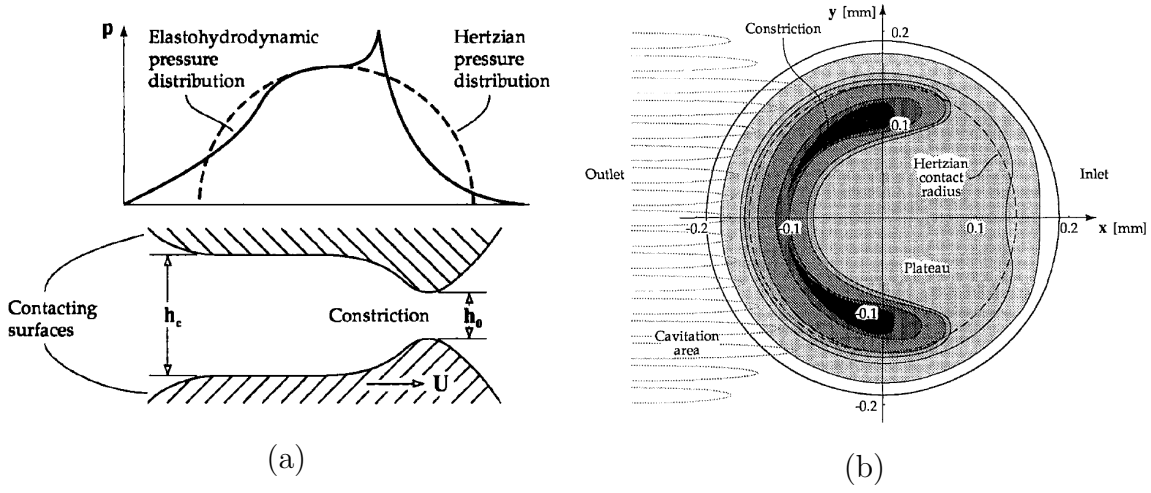

Figure 1.5: Hydrodynamic pressure distribution for an EHL contact can be seen on **(a)** as well as the location of h_c and h_{min} **(b)** depicts a schematic of the "horseshoe" effect [3].

by the asperities and friction increases [2]. Typical range for mixed lubrication is from $1 \leq \lambda \leq 3$ [8, 2].

1.1.6.4 Boundary Lubrication

Boundary lubrication occurs when interacting surfaces experience asperity contact and minimal fluid film lubrication, leading to high friction. Lubrication in this regime is a complex process and is controlled by lubricant additives that form protective films, called tribofilms, on the contacting surfaces [8]. Specifically, additives form a molecular layer that bonds to solid surfaces through adsorption (physical or chemical) and/or tribochemical reactions which help reduce friction and wear between interacting surfaces compared to dry contact conditions [1, 8]. This lubrication regime is characterized by $\lambda < 1$ [8, 2], meaning that surface roughness is larger than film thickness. Boundary lubrication can be the result of high loads or very low sliding speeds which causes the load support by the lubricating film to be negligible

[2].

1.2 Motivation

1.2.1 Tribological Differences Between ICEVs and EVs

Internal combustion engine vehicles (ICEVs) have been able to take advantage of decades of tribological research to optimize material and lubrication needs. Although, some of those advancements in tribological technology may be transferred over from ICEVs to electric vehicles (EVs), differences in tribological knowledge and performance of components for EV applications exist.

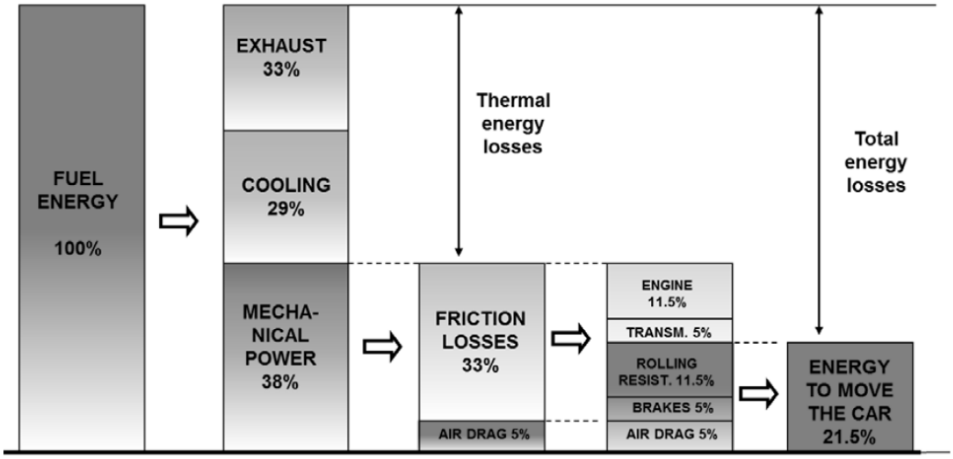

Figure 1.6: Passenger ICEVs energy breakdown; tank-to-wheel calculations [4].

Most previous studies of automotive applications focus on systems and operating environments of ICEVs. For example, the automotive bearing literature mainly focuses on applications for ICEVs [6]. Yet, the efficiency of passenger vehicles using ICEs only reaches about 21% efficiency with the remainder being lost energy [4]; see Fig. 1.6. In addition to the low energy efficiency of ICEVs, manufacturers

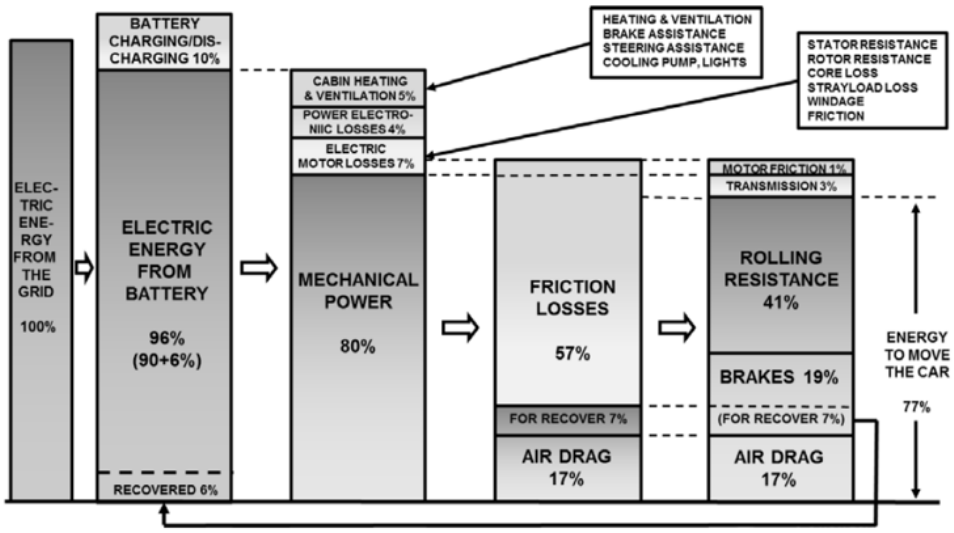

Figure 1.7: EV energy breakdown; grid-to-wheel calculations [4].

and governments around the globe are pursuing the introduction of EVs to reduce carbon emissions as well as dependency on fossil fuels which will have economic and environmental significance [4, 5]. In fact, countries around the world have made public commitments to phase out ICEVs and move to zero emissions vehicles [5]; see Fig. 1.8. Efforts have led to developments and advances in lubrication and material for EVs but energy and material losses as a result of friction and wear remain an important area of interest [4]. That is, although EVs use 77% of their energy to move the vehicle and thus making them more efficient than ICEVs, EVs still have to use 57% of the total energy to overcome friction [4]; see Fig. 1.7. In addition to energy losses, the electric motors (EMs) used to power EVs experience tribological challenges that further impact their performance and life. Consequently, research on materials and lubrication is needed to improve the efficiency and durability of all forms of transportation vehicles [4].

Year	Place	Comments
2018	Copenhagen	Any diesel car registered after this date to be banned from entering city
	Ireland	Cities to buy only ZE buses from this year
2024	Rome	Diesel vehicles banned from city center
2025	Norway	Stop new registrations of IC cars
	Paris	Ban diesel vehicles from city
	Amsterdam	IC ban proposed
	London	Extended zero-emission zone
2030	Paris	Ban on all IC vehicles from city
	India	Aim to sell only EVs from this date
	Ireland	Stop sales of IC
	Israel	Ban imports of petrol and diesel cars
	Brussels	Diesel vehicles to be banned
	Netherlands	Zero emissions only from this date
	France	Stop sales of new petrol and diesel vehicles
2032	Scotland	Stop sales of petrol and diesel cars
2035	Taiwan	Ban on sales of nonelectric PTW
2040	Taiwan	Ban on sales of non-EV 4 wheelers
2040	UK	"Majority" of new cars and vans to be zero emissions
2050	UK	"Almost every" car and van to be zero emissions
	US states: CA, CT, MD, MA, NY, OR, RI, VT	Aim to make all new passenger vehicle sales ZEV by 2025
	Canada province of Québec	Aim to make all new passenger vehicle sales ZEV by 2025
Non specific	China	Aim to phase out IC
	Germany	Aim to phase out IC, but some cities have introduced diesel bans

Figure 1.8: Governments committing to restrictions on ICEVs [5].

1.2.2 Tribological Losses in EMs

EVs are emerging as the future of transportation as the market shifts from ICEVs to electrification [4, 5, 3]. Although EVs are more energy efficient than ICEVs, energy losses in electric motors (EMs) are still considerable [6, 9]. Mechanical losses in EMs mainly derive from friction in bearings [6, 10, 11]. Further, about 40-60% of early EM failures are said to be premature bearing faults [12, 9], with most failures being due to improper lubrication [12]. Grease is used in 80–90% of rolling bearings [6, 13] and, consequently, failed grease lubrication is the predominant cause of EM

bearing failure [14, 15, 16]. Another source of premature bearing failure that adversely affects EM life is exposure to electrical environments like those found in EVs [9]. Therefore, it is important to understand how tribology can ensure the success of the electrification of the transportation industry. Formulating greases for EV applications is a particular challenge because of key differences between the environment and operating conditions in EVs and those experienced by greases in traditional ICEVs, particularly, speed, temperature and materials. These conditions are also experienced by greases in industrial EMs.

1.2.3 Challenges for Grease in EM Bearings

1.2.3.1 Speed

First, EMs in industrial applications and EVs are operated at high speeds. EMs deliver consistent torque over a broad range of speeds [5]. As a result, high motor speeds are common during operation. However, grease does not perform the same during low speeds and high speeds which presents an interesting lubrication challenge.

Grease lubrication is very dependant on speed and can exhibit inverse Stribeck behavior where friction is low at low speeds [17, 18]. This deviation from the behavior of lubricating oils is most significant at low λ ratios, i.e. small film thickness to effective surface roughness ratios [17]. In addition, at low speeds or nominal boundary conditions, friction is determined by grease thickener alone and is lower than that predicted for base oil [17, 19, 20]. Grease film thickness is larger than calculated for a base oil at low speeds, and the same or lower than calculated at higher speeds [10, 21, 22, 23, 24, 25, 26].

Grease behavior changes at high speeds. Increasing speed increases centrifugal force and mechanical work which have a significant impact on grease flow, structure and bleeding properties [7]. With increasing speed, grease life decreases [7]. Therefore, the wide range of speeds expected for EMs introduces additional challenges

when selecting or designing greases for EV or industrial applications.

1.2.3.2 Temperature

High EM temperatures are another challenge for grease lubrication. Although some increase in temperature can be beneficial because it helps grease bleed and thus resupply lubricant to the bearing contact track [21, 27], high temperatures can also generate harsh operating environments. EM high rotor speed ranges generate heat [6] and motors can reach operating temperatures of 150°C [28] or even 180°C [29] for some EM applications. Therefore, greases used in EM bearings can experience thermal degradation in the form of oxidation and decreased lubricating capabilities as a result of EM operating environments [14, 15, 16]. More specifically, grease can suffer thermo-oxidation degradation as a result of high temperature during bearing operation [14] and at temperatures $>$ 120°C, oxidation ages grease which affects its lubricity and decreases grease life [13, 7]. Note that aging will affect the rheological properties of the grease differently depending on its formulation [19]. For very high temperature cases, grease will experience severe degradation causing the grease to lose its consistency; maximum temperature is given by the dropping point of the grease [7]. The combined result of high temperatures and high speeds is the degradation of grease which reduces lubricating capabilities and adversely affects film formation, leading to ineffective lubrication [7, 14].

1.2.3.3 Materials

Another challenge for grease lubrication of EMs is that the materials of bearings may differ from those in traditional applications. Specifically, many EM bearings have ceramic components that act as insulators to mitigate issues related to stray current. Stray current can damage both the bearing and the grease quality, as well as generate heat which can cause localized melting of metal surfaces, cause pitting, break particles loose and embrittle materials [30, 31]. Current discharge

also causes grease degradation by thermal-oxidation and evaporation of the base oil and additives which then makes grease rigid [30]. Grease that is electrically conductive can amplify these effects and accelerate bearing damage [31]. The adverse effects of stray current on bearing failure will be more prevalent as EVs become a larger portion of the transportation sector [9]. Therefore, it is necessary to better understand how the electric environment influences EM bearing/grease systems [9] and develop tribological knowledge of non-traditional bearing materials operating in EM environments.

The most common ceramic material used for such applications is silicon nitride. Silicon nitride is suitable for bearings due to its mechanical properties across wide temperature ranges, electrical insulation, thermal shock resistance, excellent fracture toughness, wear resistance, long life and reliable low maintenance operation [32, 33]. Silicon nitride serves as a bearing insulator [30] that disrupts stray current in EMs and thus prevents grease thermal degradation and melting of material that leads to wear. Often, silicon nitride is used in hybrid bearings that consist of ceramic rolling elements and traditional steel raceways [30]. Hybrid bearings have been found to last longer than predicted based on the Lundberg-Palmgren theory [34] and grease life with hybrid bearings was found to be up to four times longer than with traditional all steel bearings [30]. However, there are issues associated with the use of ceramic bearing elements, particularly related to lubricant additives. For example, phosphorus-based additives were found to not react with silicon nitride as they would with steel so the tribofilms formed were not effective in improving silicon nitride bearing life [35, 36, 37]. Another potential issue is that hybrid bearings experience higher Hertzian contact stress than all steel bearings under the same applied load [34]. High contact stress is the result of differences in material hardness. Ceramic material has greater hardness than steel and thus ceramic deforms less at the contact site which results in a smaller contact area than an all steel configuration. A load applied to a smaller contact area will result in greater contact pressure than the same load

applied to a larger contact area; pressure develops stress.

1.2.4 Grease Composition

The above mentioned challenges with grease lubrication in EMs can be partially addressed through design or selections of greases specifically for EM environments. Thickener type, base oil type and viscosity all have significant effects on film thickness and friction for grease lubricated rolling/sliding contacts [17, 18, 19, 38]. Greases are continually changing as formulators and designers seek to optimize lubrication in different operating environments while remaining compatible with component materials. For example, recent studies in grease lubrication research have used nanotechnology to create novel additives for grease formulations that improve lubricity and grease life [6, 39, 40, 41]. Another study focused on extending EM bearing life by reducing grease degradation and found this can be achieved with the use of an antioxidant and high-temperature composite grease formulation [14]. Continued research and development of grease formulation is crucial because grease behavior is extremely application dependent [27].

1.2.5 Formulation Importance and Study Findings

Grease optimization often focuses on identifying the best combination of base oil and thickener for EM applications. Studies have evaluated the lubrication mechanisms associated with synthetic or mineral base oil with urea or lithium thickener. For instance, an ester-polyurea grease used for EMs with silicon nitride ceramic rolling elements was found to have excellent life, resist high operating temperatures and withstand high speeds experienced in the motor [30]. Synthetic base oils resist higher temperatures while generating low fiction and improve service life [6, 42]. Although lithium thickened greases are currently the most widely used [13], some studies suggest urea thickened grease may generate lower friction, greater film thick-

ness and have a closer correlation to typical Stribeck behavior [17, 18]. A study comparing custom polyurea and lithium thickened greases on bearing steel was performed to characterize performance at 25, 70 and 120°C and average surface roughness of 10, 100 and 200 nm [17]. Polyurea greases were shown to have the lowest friction at low speed, average surface roughness of 100 nm Ra, and temperatures of 70 and 120°C. Further, it was reported that polyurea had thicker low-speed films than lithium greases [17].

1.3 Research Objective

Based on the current findings, it is evident that both base oil and thickener affect grease performance and that optimizing this performance for EM applications requires characterization at the conditions in which the motor will operate. Specifically, EM greases are subject to higher temperatures and may be required to function with different bearing materials than traditional applications. Here, we tested the tribological performance of four commercially available greases with formulations/additives designed for EM applications, with different combinations of mineral or synthetic base oil with lithium (complex) or urea thickeners. The study focused on lubrication of silicon nitride sliding on steel across a range of temperature and surface roughness conditions. The tribological performance of these greases and bearing materials was quantified in terms of friction and wear. Characterization included both ball-on-disk and 4-ball tests as well as an analysis of the results in terms of lubrication regimes. Finally, the four greases were evaluated based on a ranking system that emphasized priorities for EM applications.

Chapter 2

Methods

2.1 Greases

Four commercially available greases were studied, all of which were designed for EM applications, per manufacture specifications. All EM greases had a International Standard Organization Viscosity Grade (ISO VG) of 100 and a National Lubricating Grease Institute (NLGI) grade of 2, but with different combinations of thickener and base oil types. The specific greases studied were: synthetic-polyurea (SP), mineral-polyurea (MP), mineral-lithium (ML), and synthetic-lithium complex (SL). Note that, since the tested greases were commercially available, formulation details such as additive composition and concentration were not known. Table 2.1 provides additional information about each grease.

2.2 Ball-on-Disk

2.2.1 Material Specifications

Two types of experiments were conducted to characterize the tribological performance of the EM greases. First, a Rtec Instruments Multi-Function Tribometer

EM Grease	**Acronym**	**Base Oil Viscosity at 40°C (cSt)**	**Base Oil Viscosity at 100°C (cSt)**	**Base Oil Density at 15°C (g/cm^3)**	**Dropping Point (ASTM D2265 °C)**
Synthetic-polyurea	SP	100	14	0.85	250
Mineral-polyurea	MP	100	12	0.88	260
Mineral-lithium	ML	100	11	0.93	180
Synthetic-lithium complex	SL	100	14	0.85	260

Table 2.1: EM grease specifications.

equipped with a temperature chamber was used to perform unidirectional sliding ball-on-disk tests, illustrated in Fig. 2.1a. In those tests, a silicon nitride ceramic bearing ball with a 9.525 mm diameter and an average surface roughness (Ra) of 20 nm were used. The ceramic balls met grade 5 quality specifications. The flat disk had a 50.8 mm diameter and was made of hardened 52100 steel. An Allied High Tech Metprep 3 polisher was used to polish the disks with the use of a silicon carbide abrasive pad in water suspension for non-directional surface finish. The disks were polished to achieve a final average surface roughness of 10, 35, 60, 120 or 200 nm. Based on the ball and disk roughness, average composite roughness cases evaluated were 22, 40, 63, 122 and 201 nm. The surface roughness of the disks was measured using a Bruker DektakXT contact mode profilometer. Prior to testing, all testing surfaces were ultrasonically cleaned in heptane.

2.2.2 Test Parameters for Ball-on-Disk

Ball-on-disk test parameters closely adhered to ASTM D5707-16 with some modifications to capture key conditions expected in EM environments, specifically, bearing

material, temperature and surface roughness. The load was 10 N, corresponding to a maximum Hertz contact pressure of 1.2 GPa, and the sliding speed was 250 mm/s. Temperatures tested were 40, 100 and 150°C. For each test, about 500 mm^3 (pea size amount) of grease was applied to lubricate the samples. A grease scoop was employed for tests at 40°C to avoid starvation by continuously pushing the grease back onto the track [17, 18, 22, 23]. All tests were run to 400 m total sliding distance and each test condition was repeated three times.

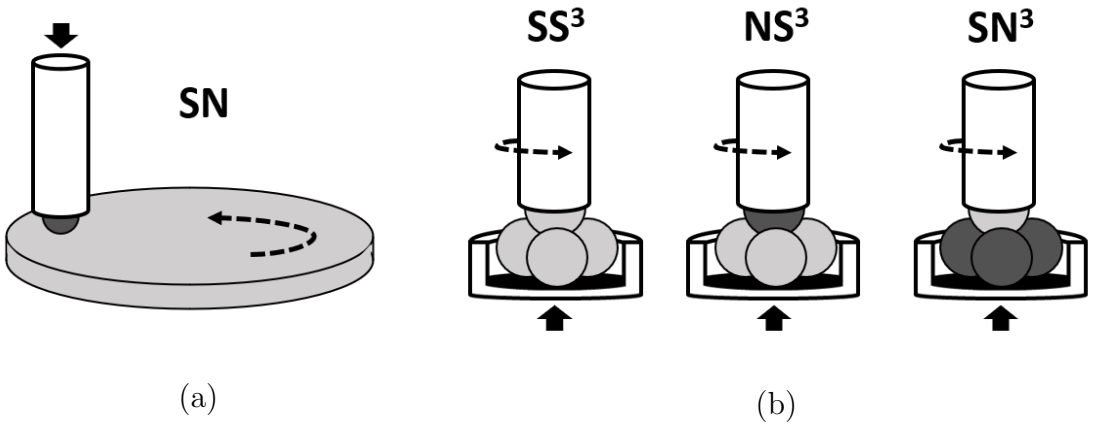

Figure 2.1: Greases were characterized using two test configurations: **(a)** Ball-on-disk and **(b)** 4-ball. The tests were performed with various combinations of steel (S) and silicon nitride ceramic (N) samples.

2.2.2.1 Grease Scoop

Early sets of ball-on-disk tests at 40°C displayed large friction spikes. That is to say, at first, the test appeared to be performing in steady state in terms of friction but, after operating for about 100 meters, a large spike in friction would emerge (see Fig. 2.2a). The large spike in friction was determined to be due to starvation because if grease was manually re-introduced onto the sliding track, the coefficient of friction would drop drastically.

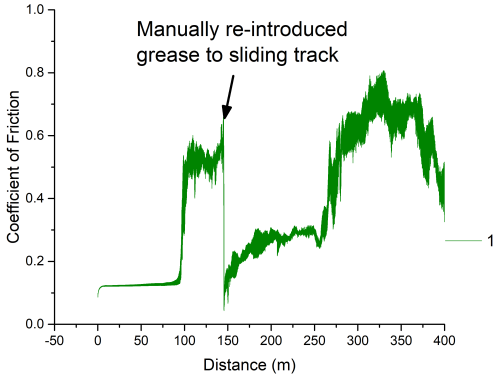

(a)

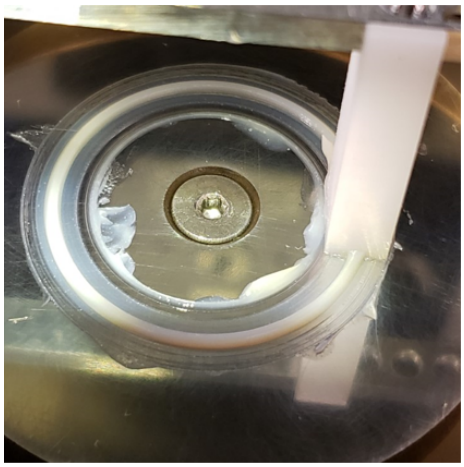

(b)

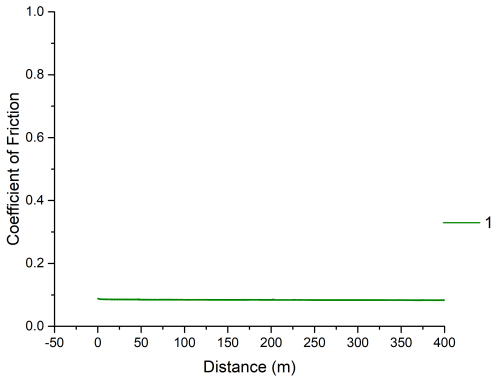

(c)

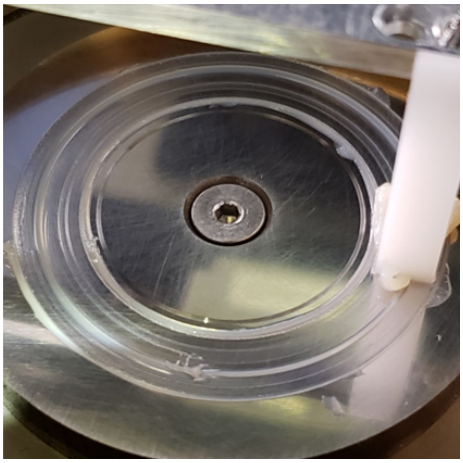

(d)

Figure 2.2: Starvation can be seen on the friction plot **(a)** as well as a drastic drop in friction once grease was manually re-introduced onto the track. **(b)** The grease scoop prevents starvation by funneling the displaced grease back onto the track and **(c)** thus preventing spikes in friction. With the use of the grease scoop system, grease is maintained on the sliding track throughout and until **(d)** the end of the ball-on-disk test.

When using grease for lubrication purposes, starvation can settle in for various reasons. Starvation refers to the lack of a lubricating film between the contact points of interacting bodies. This phenomenon occurs when operating conditions allow grease to be displaced away from the contact track with not enough time to replenish the inlet of the contacts with lubrication and thus, starvation begins to set in and film thickness significantly decreases. If grease distribution and reflow is not controlled, contact starvation can occur at low speeds [17, 7, 43, 44] as well as at low temperatures at which greases have little to no bleeding.

To control and prevent starvation conditions, a grease scoop system was designed [18, 22, 17]. The grease scoop design consisted of two components; both components were drafted using computer aided design software. One component was the bracket

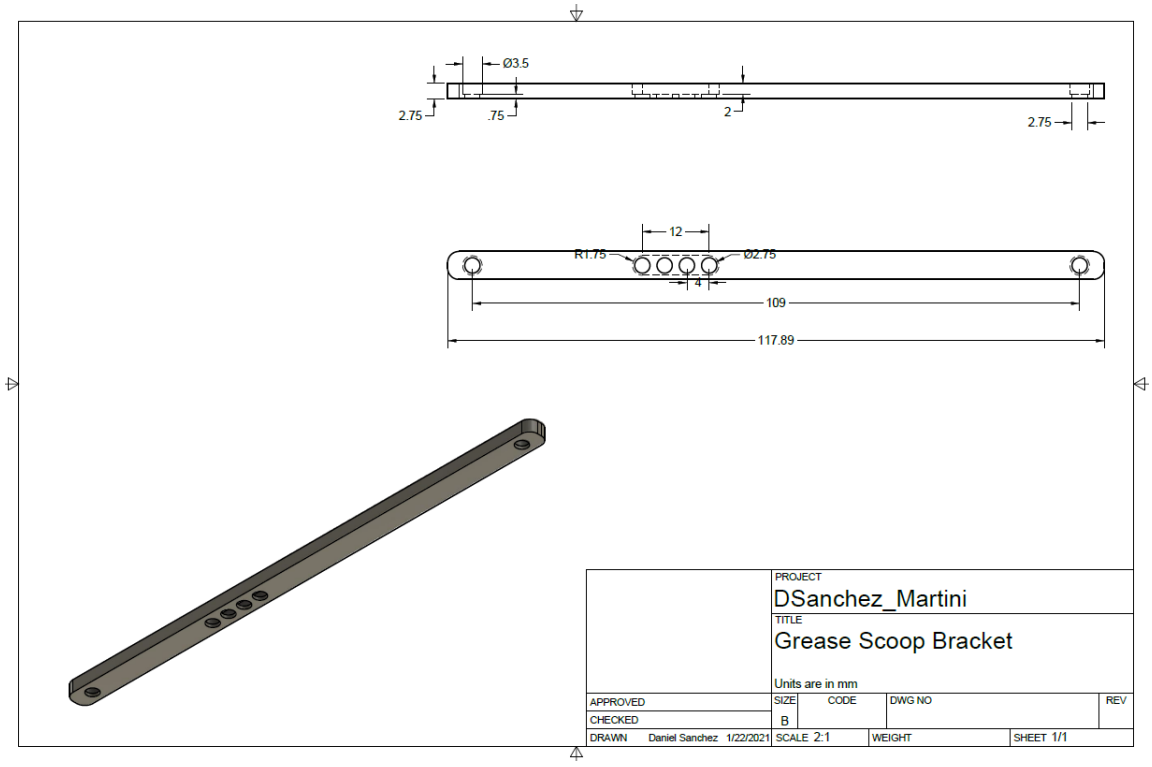

Figure 2.3: Bracket design specifications for grease scoop.

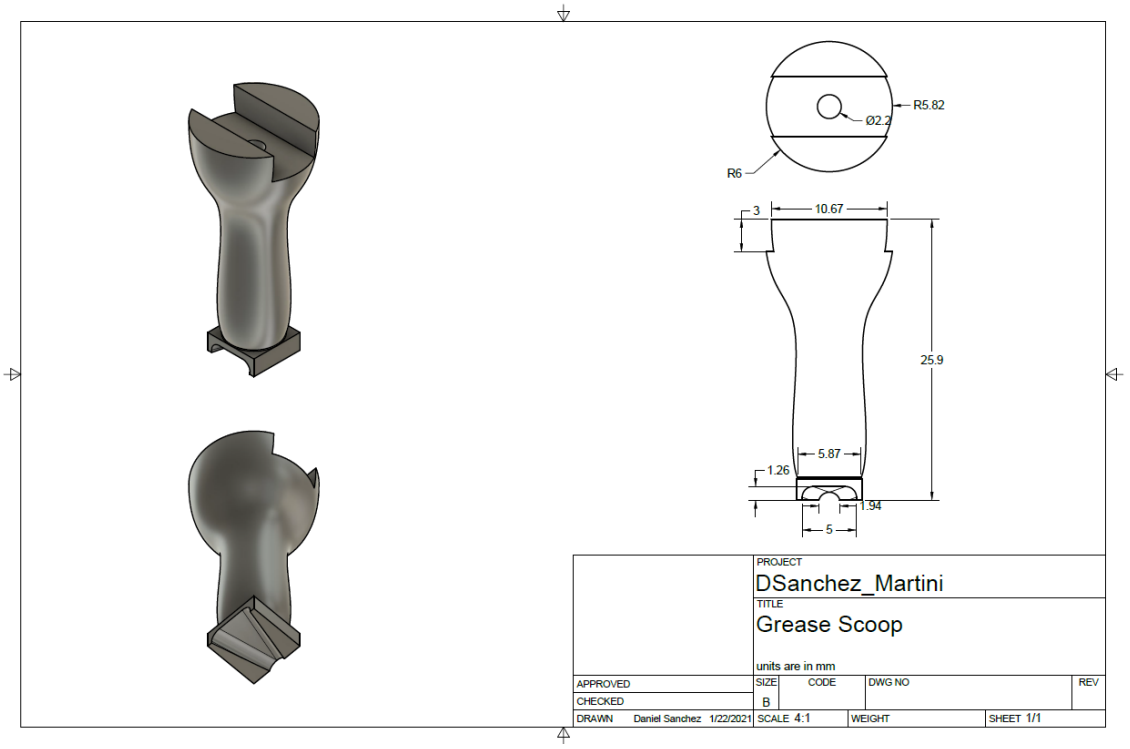

Figure 2.4: Grease scoop design.

(Fig. 2.3) that would mount directly onto the existing instrument configuration and also serve as a mounting point for the actual grease scoop. The bracket was designed with four different mounting locations to accommodate different testing radii. The second component, which contains the key functionality of the design, is the grease scoop (Fig. 2.4). At its base, the grease scoop component consists of a tapered channel that provides a funneling effect to guide the dispersed grease back to the sliding track.

With the design set, for fast prototyping purposes, the parts were first 3D printed. A final product was then machined to desired specifications (Fig. 2.5a). The bracket was machined out of 6061 aluminum; this material was chosen for the bracket because of its machinability, high strength, corrosion resistance and low cost. Poly-

tetrafluroethylene (PTFE) was used for the grease scoop because of its low friction and high-wear resistance.

The grease scoop was successfully mounted onto the tribometer configuration without for further modifications (Fig. 2.5b). As a result, the grease scoop system was able to replenished the sliding track with grease from the start (Fig. 2.2b) to the end (Fig. 2.2d) of the test. Hence, starved lubrication conditions were prevented and friction spikes due to starvation avoided (Fig. 2.2c).

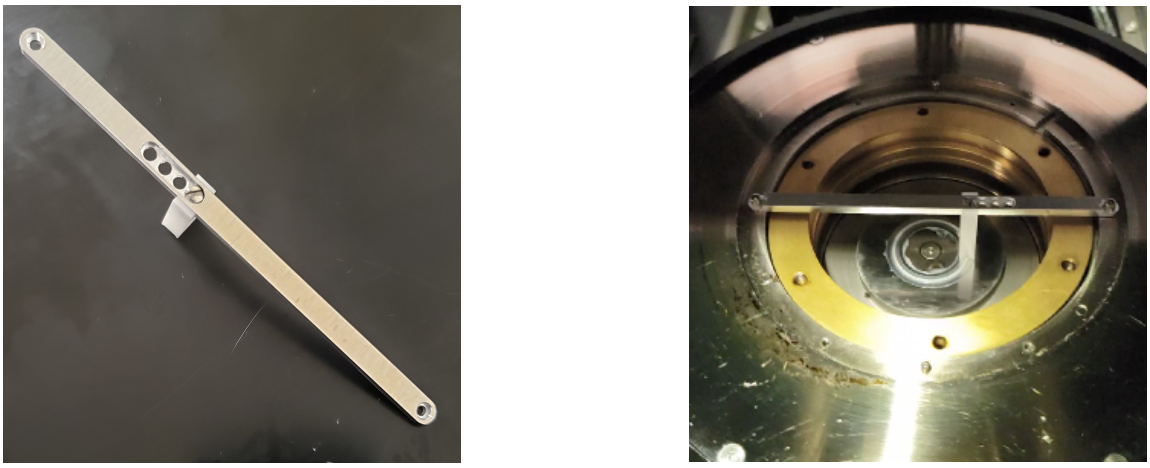

(a) (b)

Figure 2.5: **(a)** Machined components (PTFE grease scoop bolted on the aluminum bracket). **(b)** Grease scoop system mounting location on the temperature chamber along with the rest of the tribometer configuration.

2.3 4-Ball

2.3.1 Material Specifications and Configurations

Second, a Falex Multi-Specimen Test Machine was used to perform 4-ball testing, illustrated in Fig. 2.1b. The 4-ball tests enabled different combinations of silicon

nitride and hardened 52100 steel to be evaluated. Three different material configurations were tested:

- One steel rotating element on three steel stationary elements (SS^3)
- One silicon nitride ceramic rotating element on three steel stationary elements (NS^3)
- One steel rotating element on three silicon nitride ceramic stationary elements (SN^3)

The SS^3 case resembled a traditional all steel bearing assembly and the NS^3 case resembled a hybrid bearing assembly. The SN^3 resembled an inverted hybrid bearing assembly, meaning that material typically used for the races was used as the rolling element and vice versa. All-ceramic bearings are infrequently used for standard applications, so the NN^3 configuration was not tested here.

2.3.2 Test Parameters for 4-Ball

Test parameters followed the ASTM-D2266 standard. The load was 392 ± 2 N, which corresponds to a maximum Hertz contact pressure of 4.6 GPa for the SS^3 configuration and 5.2 GPa for the NS^3/SN^3 configurations. The silicon nitride ceramic test balls met grade 5 quality specifications and had a surface roughness of 20 nm Ra. The steel balls met grade 10 quality specifications and had 25 nm Ra. The speed was 1200 ± 60 revolutions per minute for 60 minutes and the temperature was held at 75°C ± 2°C. All four greases were tested using each material configuration; the SS^3 and NS^3 results are averages of three tests and the SN^3 results are averages of two tests. Error was calculated as the difference between the maximum and minimum wear for each configuration and grease.

2.4 Wear Imaging and Wear Rate Calculations

Images captured of the worn ball surfaces were obtained using a Leica Optical Microscope (Model DM 2500M) for both test methods. For the ball-on-disk tests, wear volume was calculated per ASTM G-133-05. Specific wear rate was then calculated by dividing the volume by the load and total sliding distance. For the 4-ball test, wear scar diameters were measured per ASTM D2266-01. Those measurements were then used to calculate the wear area of the scar.

Chapter 3

Results

3.1 Ball-on-Disk Wear

3.1.1 Wear vs. Roughness

Wear rate as a function of surface roughness for all EM greases is shown in Fig. 3.1a. For smooth surfaces, the wear rates of the four greases are similar, although the lowest wear is observed for the MP. In contrast, there is more differentiation between the greases on rougher surfaces, where the ML consistently exhibits the lowest wear rate. Also, for these testing parameters, greases with mineral base oil have lower wear rate than the synthetic base greases.

3.1.2 Roughness Dependence

The sensitivity of wear rate to changes in roughness was quantified as the slope of a linear fit to the data. Although this analysis is based on an assumption that wear rate increases linearly with roughness, the approach enables direct comparison of the greases. The slope calculated from a linear fit to the wear rate vs. roughness data is shown in Fig. 3.1b. This analysis indicates that wear rate with the ML grease

is the least dependant on surface roughness. Also, of the tested greases, greases with mineral base oil have less wear-roughness dependence than the synthetic base greases.

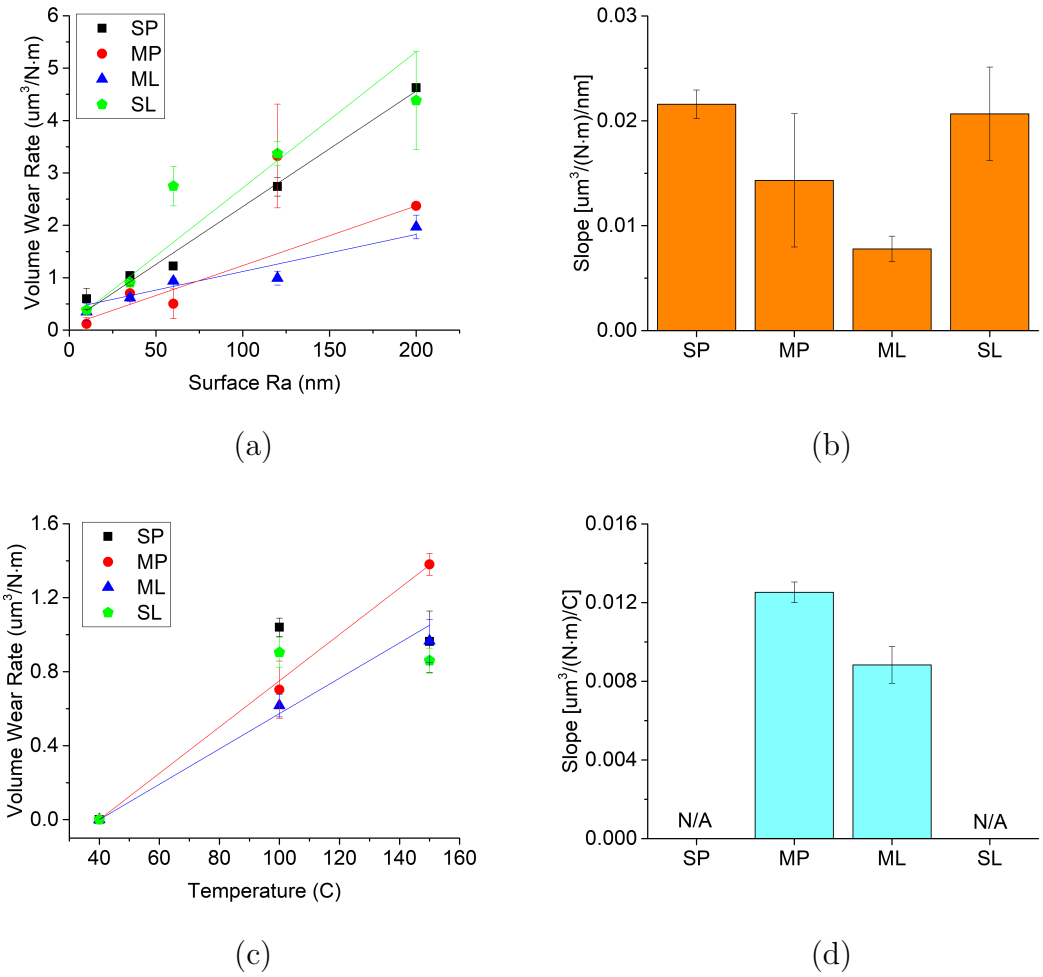

Figure 3.1: Wear results from EM grease ball-on-disk tests. **(a)** Wear rate as a function of roughness and **(b)** change in wear rate with roughness at 100°C. **(c)** Wear rate as a function of temperature and **(d)** the change in wear rate with temperature at 35 nm Ra (composite Ra of 40 nm) for MP and ML.

3.1.3 Wear vs. Temperature

Wear rates at different temperatures are shown in Fig. 3.1c. At 40°C, there is no observable wear for any of the greases. The lowest wear rate at 100°C is observed for the ML grease and, at 150°C, is found for the SL grease. Additionally, at 100 and 150°C, for the greases tested here, lithium thickened greases have a lower wear rate than their polyurea counterparts.

3.1.4 Temperature Dependence

The temperature dependence of the wear rate is very different for synthetic vs. mineral based greases. Specifically, the wear rate increases nearly linearly between 100 and 150°C for the mineral greases, but is nearly constant for the synthetics. Due to this behavior, the linear approximation cannot be used to quantify the change of wear rate with temperature for the synthetic greases. However, the linear fit was performed for the mineral greases as shown in Fig. 3.1d. The wear rate is less dependent on temperature for the ML grease than the MP grease.

3.2 Ball-on-Disk Friction

3.2.1 Friction vs. Roughness

Friction results for each grease are shown in Fig. 4.4. On average, friction increased with surface roughness for all greases (see Fig. 3.2a). Also, on most surfaces, friction was lowest for the SL grease. For the rougher surfaces, the ML also exhibited low friction behavior. For these tests, the lithium based greases had lower friction than the polyurea greases, except on the smoothest surfaces where the friction coefficient was below 0.08 for all greases.

3.2.2 Friction vs. Temperature

Friction at three different temperatures is shown in Fig. 3.2b. At 40°C, the lowest friction was exhibited by the SP grease whereas, at 100°C, the SL grease had the lowest friction. At both 40 and 100°C, the friction was lower for synthetic greases than their mineral counterparts. At 150°C, the friction coefficient was comparable for all four greases.

3.2.3 Need for Stribeck Curve Analysis

The friction trends with respect to roughness and temperature are not linear. This is primarily because both roughness and temperature affect the lubrication regime. Further, increasing temperature can promote grease bleed such that the degree of starvation decreases with increasing temperature [21]. So, the effect of these parameters on friction cannot be quantified using a simple linear fit. Instead,

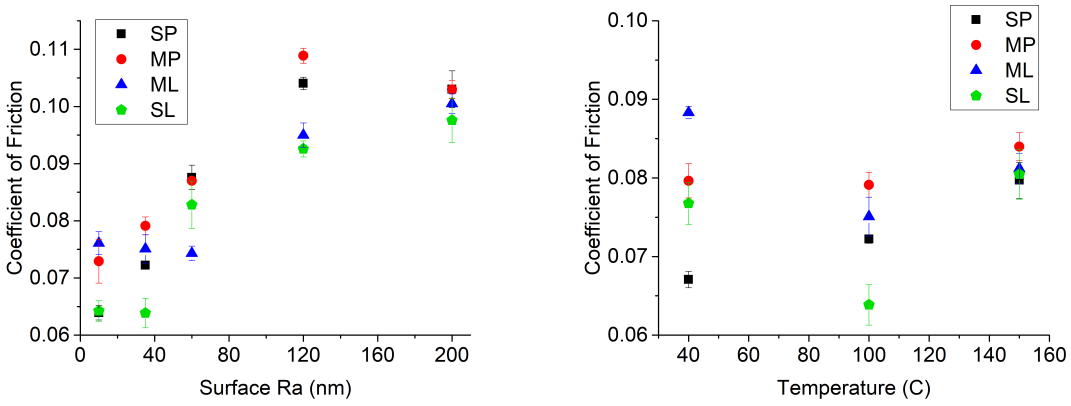

(a) (b)

Figure 3.2: Friction results from EM grease ball-on-disk tests. Friction coefficient **(a)** as a function of surface roughness at 100°C and **(b)** as a function of temperature at 35 nm Ra (composite Ra of 40 nm).

these trends will be analyzed in the context of the Stribeck curve, as discussed later.

3.3 Four-Ball Tests

3.3.1 Grease Comparison

Results from the 4-ball tests are shown in Fig. 3.3. ML had the lowest wear across all three bearing configurations. The performance of ML might be attributable to thicker lubricating films that provide more separation between interacting surfaces or better anti-wear film formation. For the SS^3 and NS^3 configurations, average wear increased as ML < MP < SP < SL. However, this trend cannot be directly explained since the 4-ball test is primarily measuring anti-wear behavior and the additive composition of these commercial greases is unknown. For the SN^3 configuration, wear was high for all four greases and large error bars precluded direct comparison between the greases.

3.3.2 Configuration Comparison

Comparing the different material combinations, for all greases, the lowest average wear was observed for NS^3, followed by SS^3 and then SN^3. The observation that wear for NS^3 was lower than that for SS^3 is consistent with previous reports that grease life with hybrid bearings is longer than with standard bearings [30]. Lower wear for NS^3 is also consistent with experimental and anecdotal observations that suggest longer lives for hybrid bearings than estimated by the Lundberg-Palmgren equations [34].

In contrast, the SN^3 configuration consistently had very high wear. This configuration also exhibited qualitatively very different behavior than the other two material pairs. As shown in the insets to Fig. 3.3, the wear scars for the SS^3 and NS^3 configurations are circular while those for the SN^3 are elliptical. The wear mechanism of the rotating elements determine and may cause non-circular wear scars of the sta-

tionary balls [45]. Therefore, the difference may be attributable to the hardness of the rotating element. For SN^3, the steel ball is the rotating element attached to the spindle (upper ball) while the three lower balls are silicon nitride. Material hardness affects material wear; a softer steel ball rotating on a harder ceramic ball causes the wear scar to elongate with increasing material deformation and thus causing relative displacement between the upper and lower balls.

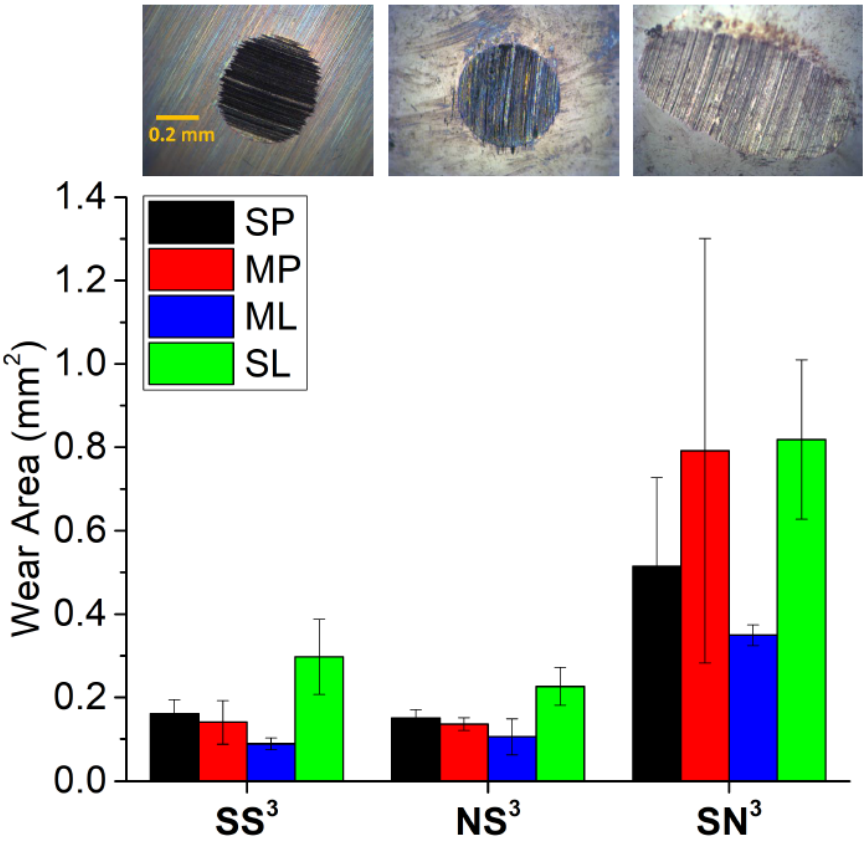

Figure 3.3: Wear area for four greases and three bearing configurations measured using the 4-ball test. Representative wear patterns (from left to right): SS^3 circular wear scar on steel ball, NS^3 circular wear scar on steel ball, and SN^3 elliptical wear scar on ceramic ball.

Chapter 4

Analysis and Discussion

4.1 Lubrication Regime Analysis

4.1.1 Lambda Ratio Calculations

The friction results shown in Fig. 4.4 suggested that changing either roughness or temperature caused a transition between lubrication regimes. The lubrication regime can be determined by the lambda ratio:

$$\lambda = \frac{h}{\left(R_{a,ball}^2 + R_{a,disk}^2\right)^{1/2}} \tag{4.1}$$

where h is the film thickness, $R_{a,ball}$ is the average roughness of the ball and $R_{a,disk}$ is the average roughness of the disk. Although the exact values of λ corresponding to transitions between lubrication regimes vary in the literature, they are often defined by $\lambda \gtrapprox 3$ for full film lubrication, $1 \lessapprox \lambda \lessapprox 3$ for mixed lubrication $\lambda \lessapprox 1$ for boundary lubrication [46, 38, 47]. However, these transition values are not absolute and studies have shown that full film or mixed lubrication is possible even in cases where λ would typically suggest boundary lubrication (e.g. $\lambda \lessapprox 1$) [47].

4.1.2 Lambda and Contact Fatigue Life

For bearings, the λ ratio also affects contact fatigue life (Fig. 4.1). Low λ ratios are associated with surface deformation and distress but those adverse effects can be mitigated by large λ ratios [3]. In the context of the conditions studied here, small surface roughness and low temperature conditions that correspond to higher λ ratios will have lower contact fatigue and longer life.

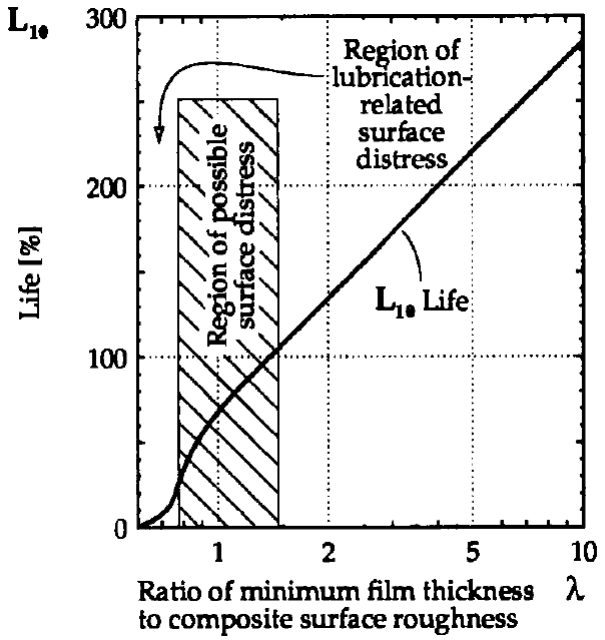

Figure 4.1: Relationship of lambda ratio to contact fatigue life [3].

4.1.3 Central Film Thickness

To calculate λ, we first had to determine film thickness. It is known that the film thickness of a grease may be larger or smaller than the film thickness for its base oil, depending on the operating conditions [17, 38]. However, there is no standard equation or method of calculating grease film thickness that is applicable

for all conditions. Therefore, as a first order approximation, we calculated film thickness using the Hamrock and Dowson equation [3] for central film thickness with parameters for the base oil:

$$h \approx h_c = 2.69R\left(\frac{U\eta}{ER}\right)^{0.67}(\alpha E)^{0.53}\left(\frac{W}{ER^2}\right)^{-0.067}(1-0.61e^{-0.73k}) \tag{4.2}$$

where, U is the speed, R is effective radius, E is effective elastic modulus, α is the pressure-viscosity coefficient, η is the ambient viscosity, W is the load, and $k = 1$ for a spherical geometry. Most of these parameters are constant for the ball-on-disk tests. However, the ambient viscosity and pressure-viscosity coefficient were calculated for each test based on the rheological properties of the base oil and the temperature. Table 4.1 summarizes the film thickness and λ ratio for each EM grease, temperature and roughness case considered in this study.

Temperature	°C	40	100	100	100	100	100	150
Composite Roughness	nm	40.3	22.4	40.3	63.3	121.7	201	40.3
SP	h_c	117	28.3	28.3	28.3	28.3	28.3	13.7
	λ	2.89	1.27	0.70	0.45	0.23	0.14	0.34
MP	h_c	151	27.8	27.8	27.8	27.8	27.8	11.3
	λ	3.74	1.25	0.69	0.44	0.23	0.14	0.28
ML	h_c	142	26.9	26.9	26.9	26.9	26.9	11.0
	λ	3.52	1.20	0.67	0.42	0.22	0.13	0.27
SL	h_c	117	28.3	28.3	28.3	28.3	28.3	13.7
	λ	2.89	1.27	0.70	0.45	0.23	0.14	0.34

Table 4.1: EM grease calculated film thickness (h_c in nm) and lambda (λ) ratio at all tested composite roughness and temperature combinations.

4.1.4 Lambda and Stribeck Curve

The friction measured from the ball-on-disk tests is plotted as a function of the calculated λ ratio to create a Stribeck curve in Fig. 4.3. The large λ cases correspond to tests run on smooth surfaces and at lower temperatures. Conversely, rough surfaces and high temperatures lead to small λ ratios. The general shape of the Stribeck curve in Fig. 4.3 indicates that our tests included the mixed regime, where friction decreases with λ, and the full film regime, where friction increases with λ.

4.1.5 Friction in Different Lubrication Regimes

The greases clearly exhibit full film at larger lambda ratios. In this regime, the lowest friction was exhibited by the SP and SL (synthetic greases). The mixed regime is clearly observed at small λ ratios. Here, as composite roughness increases, λ values decrease, and friction tends to increase. In mixed lubrication, the lowest friction was observed for the ML and SL (greases with lithium thickener). Across most of the lubrication regimes measured, SL had the best friction performance.

4.1.6 Full Film and Mixed Lubrication Transition Lambda

The transition between the full film and mixed lubrication regimes is important because both friction and wear are higher in the mixed regime due to asperity contacts in the interface. Therefore, it is desirable to remain in the full film regime as long as possible. To identify the λ ratio at which the full film-mixed transition occurs for each grease, we found the intersection of a linear fit to the data in the mixed regime and a linear fit to the data in the full film regime. The two largest λ ratios for each grease were fit for full film and the three smallest λ ratios were fit for the mixed regime. Fig. 4.2 shows the linear fits and their intersection which was identified as the transition lambda (λ_t). The λ_t values for each grease were found to be: SP at $\lambda_t = 0.48$, MP at $\lambda_t = 0.47$, ML at $\lambda_t = 0.37$, and SL at $\lambda_t = 0.58$.

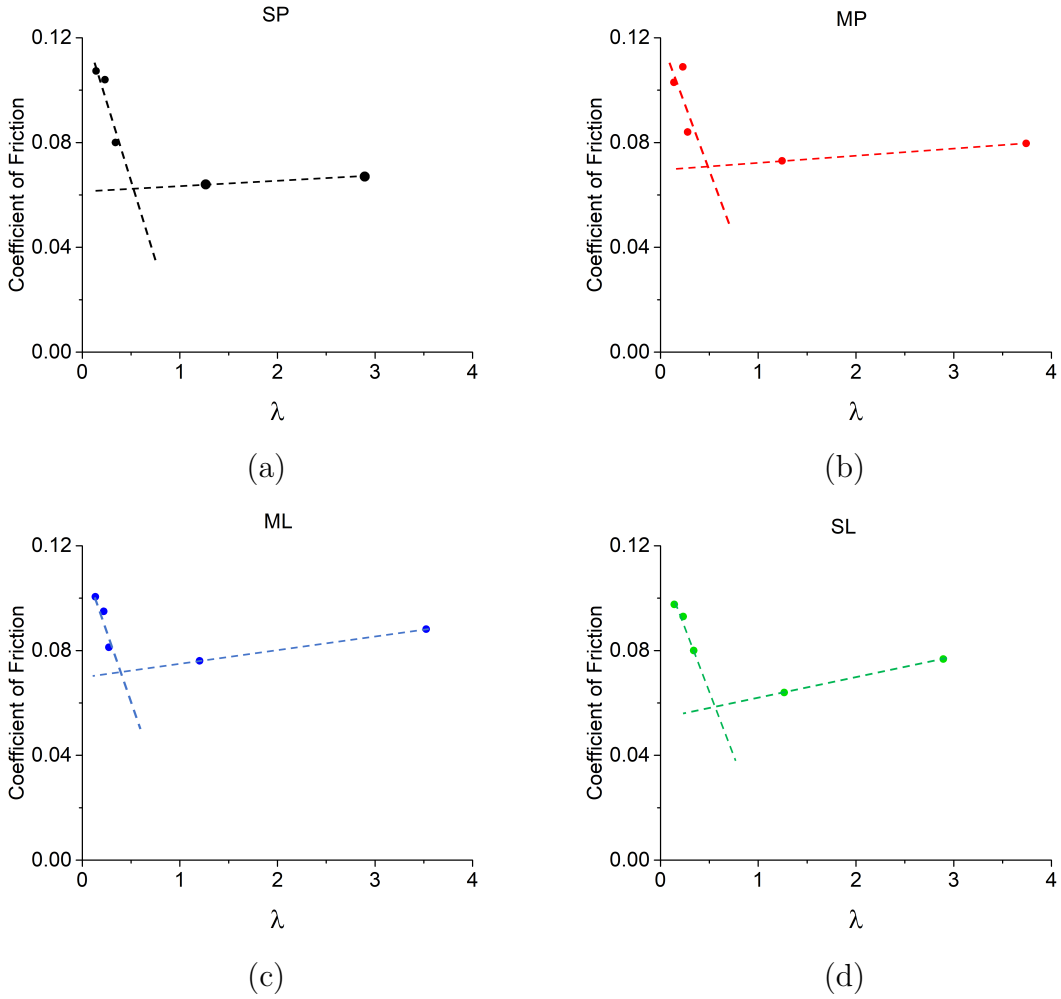

Figure 4.2: Independent linear fits performed for the mixed and full film regimes for **(a)** SP, **(b)** MP, **(c)** ML, **(d)** SL. The intersection of the two lines corresponds to the transition lambda λ_t.

4.1.7 Transition Lambda Comparison

The ML grease had the lowest λ_t, indicating that the interface would remain in the full film regime the longest with increasing temperature or roughness. However, it is important to note that ML also has higher friction in this transition region. So,

ML's lower λ_t suggests the lubricant is able to maintain a thicker lubrication film than the other greases but this comes at a cost of higher viscous friction. On the other hand, SL has a larger λ_t value but considerably lower friction than the rest of the tested greases in this transition range. In fact, despite having a larger λ_t value, SL maintained lower friction at most test conditions. This analysis shows there is a compromise between low friction in full film lubrication and how long the interface will remain in that regime before the onset of mixed lubrication.

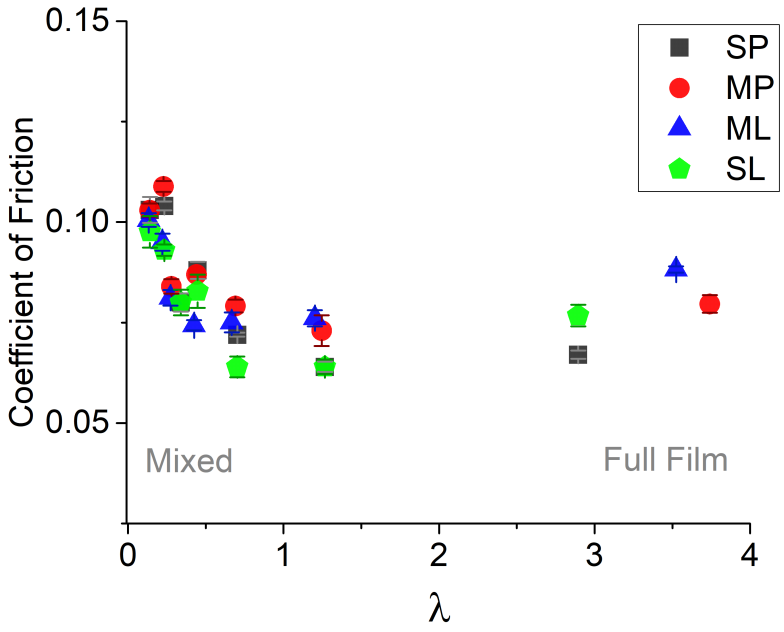

Figure 4.3: Stribeck curve based on measured friction and calculated λ ratios for four greases tested across all roughness and temperature conditions.

4.2 Predicted Lubrication Regime Transitions

4.2.1 Approach Motivation

The λ ratio determines lubrication regime as well as contact fatigue. In our study, this critical ratio is determined by surface roughness, grease properties and temperature. So, for a given grease, roughness and temperature, the λ value can be calculated and the conditions at which the lubrication regime transitions to mixed can be predicted.

4.2.2 Details of the Approach and Prediction Results

Surface roughness affects this calculation directly, as it appears in the denominator of Eq. 4.1. Temperature indirectly affects the film thickness as calculated using Eq. 4.2 through its effect on η and α. The grease itself determines the values of η and α and their temperature dependence.

To predict λ for any temperature T, we need to first fit available grease data for both the ambient viscosity and pressure-viscosity coefficient. For the pressure-viscosity coefficient ($\alpha(T)$), a linear fit was employed as can be seen on Fig. 4.4a. Ambient viscosity ($\eta(T)$) required the Vogel equation [3] to fit the data (see Fig. 4.4b). The Vogel equation can be defined as:

$$Vogel\ (\eta) = ae^{\frac{b}{T-c}} \tag{4.3}$$

where $a,\ b,\ and\ c$ are constants and T is temperature. Note that c needs to have the same units of temperature as T. As a result, from the fitted $\alpha(T)$ and $\eta(T)$ equations, values were interpolated or extrapolated for any temperature. This approach thus enabled λ to be calculated directly using the equations for $\alpha(T)$ and $\eta(T)$, combined with Eqs. 4.1 and 4.2.

This analysis was performed for each grease at temperatures ranging from 30 to 200°C and composite roughness values from 20 to 200 nm Ra. The predicted λ

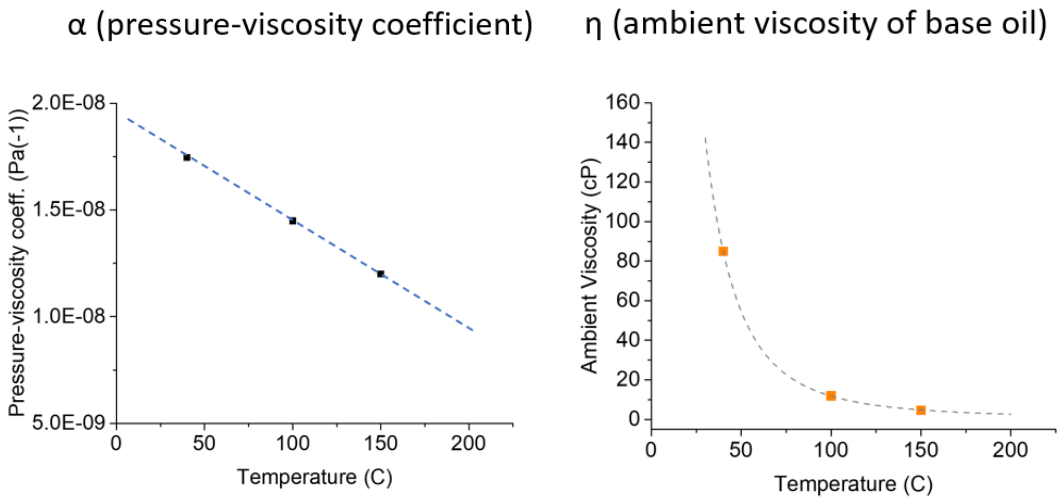

(a) (b)

Figure 4.4: Temperature dependent properties calculated by fitting available grease data. Where **(a)** depicts the linear fit for the pressure-viscosity coefficient and **(b)** depicts the ambient viscosity fitted to the Vogel equation.

values are shown as color contour plots in Fig. 4.5. Also shown are horizontal planes corresponding to λ_t, the ratio at the transition between mixed and full film lubrication, calculated from the friction data for each grease in Fig. 4.3. The intersection between this plane and the surface predicted as described above indicates the temperature and surface roughness at which the interface will transition from full film to mixed lubrication. Such an approach can be used as part of the design process to guide selection of a grease, surface roughness specifications or prescribed limits on operating conditions.

4.3 Grease Evaluation

The four greases evaluated in this study exhibited varying levels of performance at different surface roughness and temperature conditions. These observations are

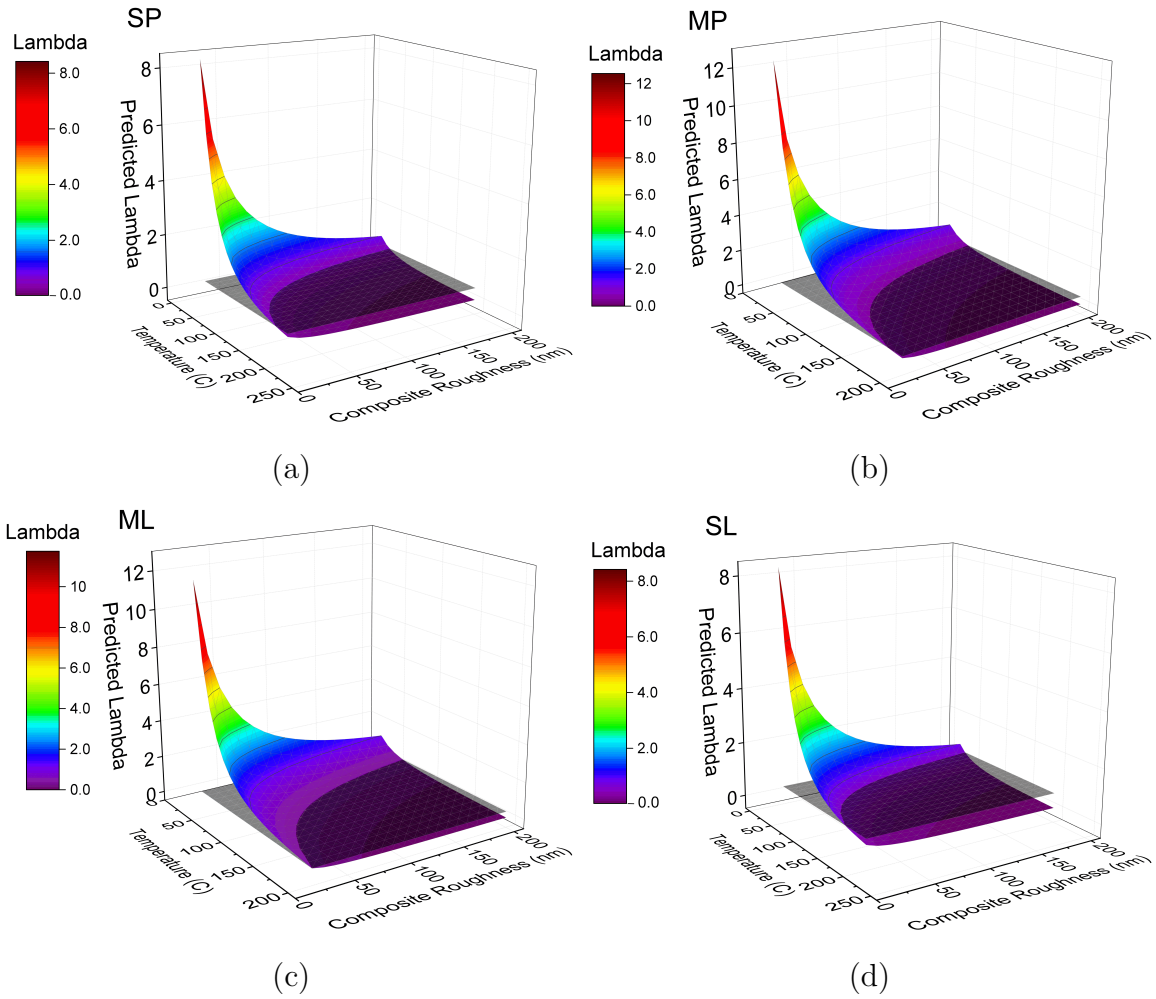

Figure 4.5: Contour plots with predicted λ ratios for each of the four commercially available EM greases: **(a)** SP, **(b)** MP, **(c)** ML and **(d)** SL. The transition between full film and mixed lubrication (λ_t) is shown as a horizontal plane.

summarized briefly here.

4.3.1 Wear Summary

As observed in Fig. 3.1a, MP had the lowest wear rate on smooth surfaces while ML had the lowest wear on rough surfaces. ML was also found to exhibit the least dependence of wear rate on surface roughness. On average, greases with mineral base oil had lower wear rate and roughness dependence than the synthetic base greases. In high temperature tests (150°C), the lowest wear rate was found for the SL grease. Also, the wear rate of the synthetic greases did not change with temperature at high temperatures, while an increase in wear rate with temperature was observed for the mineral greases. In the 4-ball tests, ML had the lowest wear across all the various bearing configurations. For the SS^3 and NS^3 configurations, average wear increased as ML < MP < SP < SL. Larger wear rates increase material debris which can have implications such as artificial surface roughness, reduced lubricating capabilities and abrasion/erosion, so low wear is extremely important.

4.3.2 Friction Summary

In terms of friction, on most surfaces, friction was lowest for the SL grease. For rougher surfaces, the lithium greases generally had lower friction than the polyurea greases. On very smooth surfaces, the synthetics had lower friction than the mineral based greases. In terms of temperature, at 40°C, the lowest friction was exhibited by the SP grease whereas, at 100°C, the SL grease had the lowest friction. At both 40 and 100°C, the friction was lower for synthetic greases than their mineral counterparts. The friction data was also used to determine transitions between the full film and mixed lubrication regime. This analysis showed that under these testing parameters, ML had the lowest λ_t, indicating that the interface would remain in the full film regime the longest with increasing temperature or roughness. However, ML also had

higher friction in this transition region indicating that the lubricant maintained a thicker lubrication film at a cost of higher viscous friction. In contrast, SL had a larger λ_t ratio but considerably lower friction than the rest of the tested greases in this range. Energy efficiency is related to the magnitude of friction. Mechanical component life and efficiency will be impacted by the coefficient of friction and thus, have an important role in outlining operating conditions and design limitations.

4.3.3 Grease Ranking System

While the comparisons between greases in terms of individual performance metrics are valuable, they need to be combined to determine which grease is best for a given application. Therefore, it is necessary to develop a grease evaluation and comparison method to assess these commercially available greases. Performance metrics included are low temperature (40°C) friction, low surface roughness (10 - 60 nm Ra) friction and wear, high surface roughness (120 -200 nm Ra) friction and wear, high temperature (100 - 150 °C) friction and wear, wear dependence on surface roughness and NS^3 (best represents EM hybrid bearings) wear from the 4-ball tests. The ranking system was developed with EM bearing applications in mind, so high temperature friction and wear were given twice the weight of the other metrics. The greases were ranked 1 through 4 (or 8 for high temperature parameters) where 4 (or 8) was best. The results are shown as radar plots in Fig. 4.6.

4.3.4 Ranking Results Summary

The individual rankings for each grease were also summed to give an overall score, shown next to the radar plots in Fig. 4.6. Based on the overall score, for the testing parameters used here, the two lithium greases outperformed the two polyurea greases (SL = 34 > ML = 31 > SP = 25 > MP = 22). The overall score can also be separated into a friction rating and a wear rating, both of which are reported

next to the radar plots in Fig. 4.6. In terms of friction performance, the results indicate that the synthetic greases had better overall friction performance than the mineral based greases (SL = 19 > SP = 14 > ML = 10 > MP = 7). Consistent with the overall rating, SL exhibited the best friction performance, particularly at high temperatures. However, different trends are observed for wear and the overall wear scores indicate that mineral greases outperformed their synthetic counterparts (ML = 21 > SL = 15, MP = 15 > SP = 11). The ML exhibited the best wear performance and, particularly, the least dependence of wear on surface roughness. MP and SL were tied for the second-best, but the good rating of SL was largely due to its low wear at high temperature whereas MP outperformed SL in all other wear metrics, particularly wear at low surface roughness.

The radar charts are useful to provide additional insight and enable further differentiation between greases which can prove to be very important. This is because even if a pair of greases score similarly, these two greases may be optimal for different conditions. For example ML and SL had the two highest performance scores in this study but with the use of the radar charts, it is clear SL is optimal for high temperature conditions while ML is optimal for conditions that demand optimal wear protection.

Generally, the overall ratings, along with the radar charts themselves, serve as guidelines with which a designer can evaluate each grease based on metrics important for the application being considered. However, it should be noted that long duration and high speed bearing/grease life tests would be useful as another metric to include in this type of analysis for grease evaluation for EM applications.

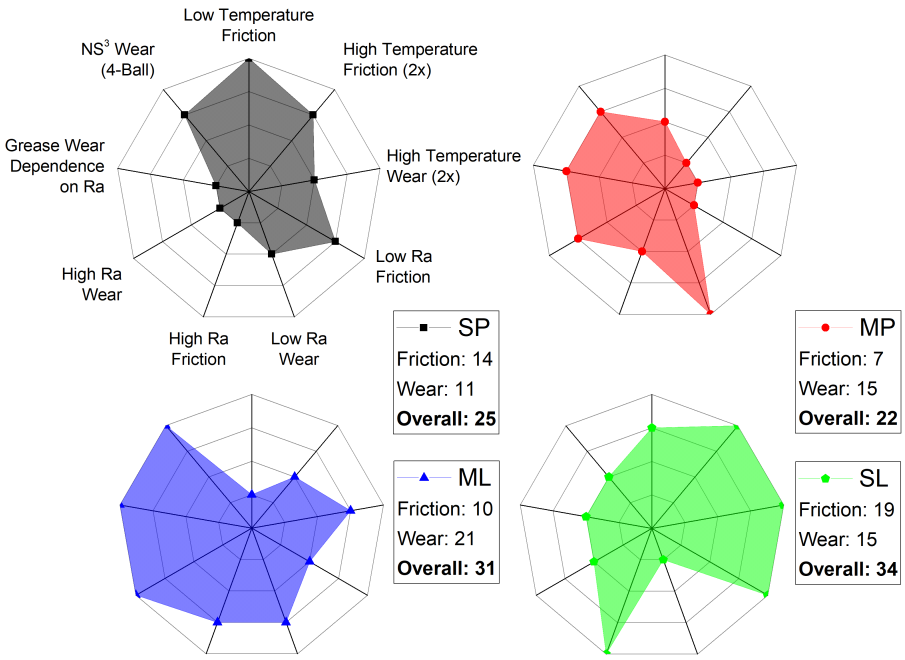

Figure 4.6: Grease ranking system based on a 1 to 4 scale (or 1 to 8 for high temperature parameters). A ranking of 4 (8) corresponds to best and 1 to worst. Low temperature is 40°C, high temperature is 100 - 150°C, low Ra is from 10 - 60 nm Ra, and high Ra from 120 - 200 nm Ra.

Chapter 5

Conclusion

5.1 Research Summary

The tribological behavior of commercially available EM greases on hybrid bearing materials was characterized and evaluated. Results showed that EM grease products have notable differences in performance across different roughness and temperature conditions. These variations in performance have important implications for lubrication and design limitations. In general, greases whose performance is least affected by changing operating conditions will be more likely to meet the tribological needs of EMs.

One parameter that has a significant affect on tribological properties is surface roughness. Rougher surfaces generally correspond to more friction and wear since they tend to have smaller local film thickness and higher pressure at asperity peaks [48, 49, 38] which result in high shear rates and stresses [17, 48, 49]. In contrast, surfaces with low roughness increase grease life and are less demanding in terms of lubrication ability since interacting smooth surfaces are more easily separated by lubricating films [13]. Yet, extremely smooth surfaces risk sudden seizure and asperities on rough surfaces may be useful for retaining lubricant [3]. Therefore,

surface roughness plays a key role in determining the performance of grease lubricated systems.

Another important parameter for grease tribology is temperature, particularly for high-speed bearings. EM grease is known to be susceptible to thermo-oxidation degradation during high temperature bearing operation [14] which can lead to grease lubrication failure and consequently, bearing failure [9, 14, 15, 16]. Temperature also influences film thickness through its affect on ambient viscosity and the pressure-viscosity coefficient. Low temperature environments may be beneficial to achieving thicker lubricating grease films and reduce wear but can increase viscous friction. Further, excessively thick and viscous grease films may cause contact starvation from poor grease bleed and lack of reflow [21] which also leads to an increase in friction [27]. On the other hand, an increase in temperature can reduce viscous friction and activate grease bleed but, under high temperatures, film thickness can decrease [44, 21, 27] to levels that may promote harsher operating conditions detrimental to grease and bearing life.

5.2 Recommendations

Managing surface roughness will be imperative to achieve efficient lubrication and prolong system life. Too rough of a surface can adversely affect lubrication and system life and too smooth of a surface can be too expensive to manufacture or possibly lead to unexpected system seizure. Therefore, optimizing surface roughness is essential and the ideal surface roughness will depend on the application being considered. The ideal surface roughness of a component will maintain low friction and wear as well as have reasonable roughness specifications for cost and manufacturing purposes.

Similarly, operating temperatures can have a significant impact on a systems tribological performance. One way to mitigate the effects of temperature is to optimize

EM grease for high operating temperatures and formulate the grease to have minimal temperature dependence. That is because grease formulations that do not compromise lubrication capabilities at high temperatures and resist thermal-oxidation are likely to be better for lubricating EM bearings. Another consideration for EMs might involve exploring different base oil viscosity and/or grease consistency. EM greases with lower viscosity base oils and/or optimal grease consistency may help manage grease shear during high-speed bearing operation which can mitigate the damage to the thickener structure and thus promote lubricating capabilities via adequate film formation, proper grease bleed and reflow. Therefore, low viscosity grease formulations may need to be explored in EM operating micro-environments.

Both temperature and surface roughness affect the lubrication regime, as quantified by the λ ratio. Ideal λ ratios during operation will be small enough to achieve low friction but not so small that there is a transition into mixed or boundary lubrication. Ideal λ ratios can also have a positive effect on bearing contact fatigue, prolong component life and improve energy efficiency. Therefore, maintaining a consistent λ ratio across temperature and roughness conditions is a key factor in component design and grease selection.

EM grease formulations also need to be optimized for hybrid bearing materials, assuming the continued use of hybrid bearings to combat stray current. Umbrella grease type products might not capture all lubrication requirements [38] and consequently may jeopardize performance and system life. Further, non-traditional bearing material and material configurations can exhibit wear mechanisms distinct from those observed in traditional steel bearings. The 4-ball test results reported here indicate the ideal hybrid bearing configuration is ceramic rolling elements on steel races (NS^3). The inverse bearing configuration, steel rolling elements on ceramic races (SN^3), generated significantly larger and abnormal wear. Additionally, the NS^3 configuration was found to have better wear performance than traditional SS^3 bearings, which has positive implications for hybrid bearings and grease life.

5.3 Final Thoughts

The results of a comprehensive set of friction and wear tests, using 4-ball tests and ball-on-disk measurements across a range of roughness and temperature conditions, showed that SL had the best overall performance under the conditions tested here (Fig. 4.6). SL provided low wear at 40 nm Ra or less and consistently maintained low friction throughout both the full film and mixed lubrication regimes. When results were analyzed in terms of friction and wear separately, it was found that synthetic greases had the best friction behavior while mineral greases had the best wear performance, with ML being best overall in terms of wear. However, ultimately grease selection will depend on the application. In the process of comparing four greases, this study also developed an approach for the λ ratio and the transition between lubrication regimes (Fig. 4.5) that may be useful as a design tool more generally.

Going forward, the tribological performance of potential hybrid bearing materials combined with grease formulations for EMs need to be fully explored under conditions that resemble the environments of the target application. This is particularly critical because tribology will play an important role enabling the electrification of the transportation industry and, through tribological research, EM bearing lubrication can be optimized for EVs as has been for ICEVs. The present study demonstrates that market-available EM grease products can vary significantly in performance, giving us insight into the effects of operating conditions and design limitations. More generally, this study is a baseline and a template for further grease research in EM environments.

Bibliography

[1] C. M. Mate. *Tribology on the small scale: a bottom up approach to friction, lubrication, and wear*. Number 6. Oxford University Press, 2008.

[2] I. Hutchings and P. Shipway. *Tribology: friction and wear of engineering materials*. Butterworth-Heinemann, 2017.

[3] G.W. Stachowiak and A.W. Batchelor. *Engineering Tribology*. Butterworth-Heinemann, 2013.

[4] K. Holmberg and A. Erdemir. The impact of tribology on energy use and CO_2 emission globally and in combustion engine and electric cars. *Tribol. Int.*, 135:389–396, 2019.

[5] P. Nieuwenhuis, L. Cipcigan, and H. B. Sonder. The electric vehicle revolution. In *Future Energy*, pages 227–243. Elsevier, 2020.

[6] L. I. Farfan-Cabrera. Tribology of electric vehicles: A review of critical components, current state and future improvement trends. *Tribol. Int.*, 138:473–486, 2019.

[7] P. M. Lugt. *Grease lubrication in rolling bearings*. John Wiley & Sons, 2012.

[8] P. L. Menezes, C. J. Reeves, and M. R. Lovell. Fundamentals of lubrication. In *Tribology for scientists and engineers*, pages 295–340. Springer, 2013.

[9] F. He, G. Xie, and J. Luo. Electrical bearing failures in electric vehicles. *Friction*, 8(1):4–28, 2020.

[10] M. Lukaszczyk. Improving efficiency in electric motors. *World Pumps*, 2014(4):34–41, 2014.

[11] J. de Santiago, H. Bernhoff, B. Ekergård, S. Eriksson, S. Ferhatovic, R. Waters, and M. Leijon. Electrical motor drivelines in commercial all-electric vehicles: A review. *IEEE Trans. Veh. Technol.*, 61(2), 2012.

[12] H. C. Walther and R. A. Holub. Lubrication of electric motors as defined by IEEE standard 841-2009, shortcomings and potential improvement opportunities. In *Proc. IEEE Petroleum Chem. Ind. Tech. Conf. Rec.*, pages 91–98. IEEE, 2014.

[13] P. M. Lugt. Modern advancements in lubricating grease technology. *Tribol. Int.*, 97:467–477, 2016.

[14] Z. Yu and Z. Yang. Fatigue failure analysis of a grease-lubricated roller bearing from an electric motor. *J. Fail. Anal. Prev.*, 11(2):158–166, 2011.

[15] P.J.L. Fernandes. Contact fatigue in rolling-element bearings. *Eng. Fail. Anal.*, 4(2):155–160, 1997.

[16] P.J.L. Fernandes and C. McDuling. Surface contact fatigue failures in gears. *Eng. Fail. Anal.*, 4(2):99–107, 1997.

[17] Y. Kanazawa, R. S. Sayles, and A. Kadiric. Film formation and friction in grease lubricated rolling-sliding non-conformal contacts. *Tribol. Int.*, 109:505–518, 2017.

[18] P.M. Cann. Grease lubrication of rolling element bearings—role of the grease thickener. *Lubr. Sci.*, 19(3):183–196, 2007.

[19] T. Cousseau, B. Graça, A. Campos, and J. Seabra. Grease aging effects on film formation under fully-flooded and starved lubrication. *Lubricants*, 3(2):197–221, 2015.

[20] T. Zapletal, P. Sperka, I. Krupka, and M. Hartl. On the relation between friction increase and grease thickener entraining on a border of mixed EHL lubrication. *Lubricants*, 8(2):12, 2020.

[21] P.M. Cann. Starved grease lubrication of rolling contacts. *Tribol. Trans.*, 42(4):867–873, 1999.

[22] N. De Laurentis, A. Kadiric, P.M. Lugt, and P.M. Cann. The influence of bearing grease composition on friction in rolling/sliding concentrated contacts. *Tribol. Int.*, 94:624–632, 2016.

[23] H. Cen, P. M. Lugt, and G. Morales-Espejel. On the film thickness of grease-lubricated contacts at low speeds. *Tribol. Trans.*, 57(4):668–678, 2014.

[24] H. Cen and P. M. Lugt. Film thickness in a grease lubricated ball bearing. *Tribol. Int.*, 134:26–35, 2019.

[25] H. Cen, P. M. Lugt, and G. Morales-Espejel. Film thickness of mechanically worked lubricating grease at very low speeds. *Tribol. Trans.*, 57(6):1066–1071, 2014.

[26] G. Morales-Espejel, P. M. Lugt, H.R. Pasaribu, and H. Cen. Film thickness in grease lubricated slow rotating rolling bearings. *Tribol. Int.*, 74:7–19, 2014.

[27] D. E. Gonçalves, A. V. Campos, and J. H. Seabra. An experimental study on starved grease lubricated contacts. *Lubricants*, 6(3):82, 2018.

[28] T. Sebastian. Temperature effects on torque production and efficiency of PM motors using NdFeB magnets. *IEEE Trans. Ind. Appl.*, 31(2):353–357, 1995.

[29] S. Hamidizadeh, N. Alatawneh, R. R. Chromik, and D. A. Lowther. Comparison of different demagnetization models of permanent magnet in machines for electric vehicle application. *IEEE Trans. Magn.*, 52(5):1–4, 2016.

[30] J. Oliver, G. Guerrero, and J. Goldman. Ceramic bearings for electric motors. In *2015 IEEE-IAS/PCA Cement Industry Conference (IAS/PCA CIC)*, pages 1–11. IEEE, 2015.

[31] A. Gonda, R. Capan, D. Bechev, and B. Sauer. The influence of lubricant conductivity on bearing currents in the case of rolling bearing greases. *Lubricants*, 7(12):108, 2019.

[32] R. C. Dante and C.K. Kajdas. A review and a fundamental theory of silicon nitride tribochemistry. *Wear*, 288:27–38, 2012.

[33] M. Volante, B. Fubini, E. Giamello, and V. Bolis. Reactivity induced by grinding in silicon nitride. *J. Mater. Sci. Lett.*, 8(9):1076–1078, 1989.

[34] E. V. Zaretsky, B. L. Vlcek, and R. C. Hendricks. Effect of silicon nitride balls and rollers on rolling bearing life. *Tribol. Trans.*, 48(3):425–435, 2005.

[35] D. W. Johnson. The tribology and chemistry of phosphorus containing lubricant additives. 2016.

[36] P.A. Bertrand. Reactions of tricresyl phosphate with bearing materials. *Tribol. Lett.*, 3(4):367–377, 1997.

[37] B. Guan, B. A. Pochopien, and D. S. Wright. The chemistry, mechanism and function of tricresyl phosphate (TCP) as an anti-wear lubricant additive. *Lubr. Sci.*, 28(5):257–265, 2016.

[38] D. Gonçalves, A. Vieira, A. Carneiro, A. V. Campos, and J. H. Seabra. Film thickness and friction relationship in grease lubricated rough contacts. *Lubricants*, 5(3):34, 2017.

[39] H. Chang, C. Lan, C. Chen, M. Kao, and J. Guo. Anti-wear and friction properties of nanoparticles as additives in the lithium grease. *Int. J. Precis. Eng. Man.*, 15(10):2059–2063, 2014.

[40] H. Qiang, L. Anling, Z. Yangming, S. Liu, and G. Yachen. Experimental study of tribological properties of lithium-based grease with Cu nanoparticle additive. *Tribol.-Mater., Surf. Interfaces*, 11(2):75–82, 2017.

[41] H. Qiang, L. Anling, G. Yachen, L. Songfeng, and K. LH. Effect of nanometer silicon dioxide on the frictional behavior of lubricating grease. *Nanomater. Nanotechnol.*, 7:1–9, 2017.

[42] G. Gow. Lubricating grease. In *Chemistry and technology of lubricants*, pages 255–268. Springer, 1992.

[43] P.M. Cann and H.A. Spikes. Film thickness measurements of lubricating greases under normally starved conditions. *NLGI Spokesman*, 56(2):21–27, 1992.

[44] P.M. Cann. Starvation and reflow in a grease-lubricated elastohydrodynamic contact. *Tribol. Trans.*, 39(3):698–704, 1996.

[45] G.A. Strunks, D.K. Toth, and C.S. Saba. Geometry of wear in the sliding four-ball wear test. *Tribol. Trans.*, 35(4):715–723, 1992.

[46] N. Walters and A. Martini. Friction dependence on surface roughness for castor oil lubricated NiTi alloy sliding on steel. *Tribol. Trans.*, 61(6):1162–1166, 2018.

[47] J. Hansen, M. Björling, and R. Larsson. Lubricant film formation in rough surface non-conformal conjunctions subjected to GPa pressures and high slide-to-roll ratios. *SCI REP-UK*, 10(1):1–16, 2020.

[48] J. Guegan, A. Kadiric, and H. Spikes. A study of the lubrication of EHL point contact in the presence of longitudinal roughness. *Tribol. Lett.*, 59(1):22, 2015.

[49] J. Guegan, A. Kadiric, A. Gabelli, and H. Spikes. The relationship between friction and film thickness in EHD point contacts in the presence of longitudinal roughness. *Tribol. Lett.*, 64(3):33, 2016.

Appendix A

Supplementary Information

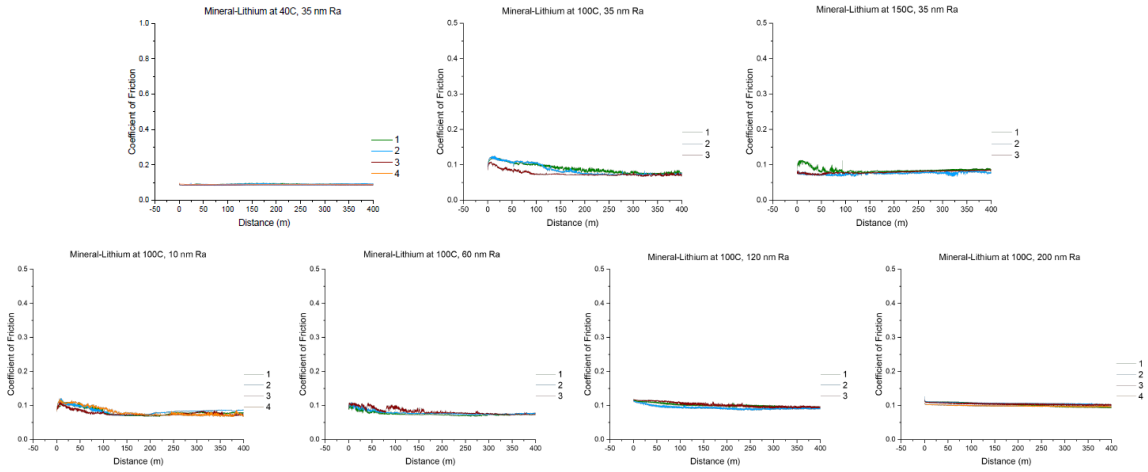

Figure A.1: Mineral-Lithium Grease: Ball on disk friction behavior for each individual test at each tested temperature.

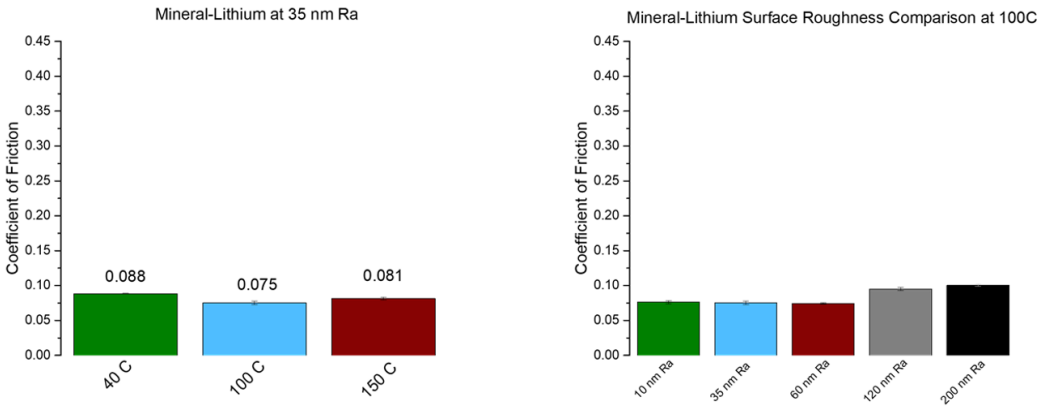

Figure A.2: Mineral-Lithium Grease: Ball on disk friction averages.

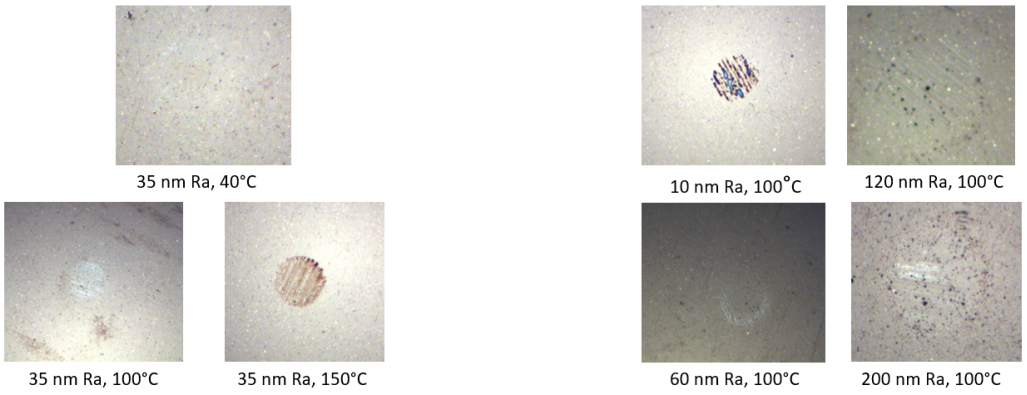

Figure A.3: Mineral-Lithium Grease: Representative wear scars for each tested condition using the ball on disk test parameters. Images are at 10x.

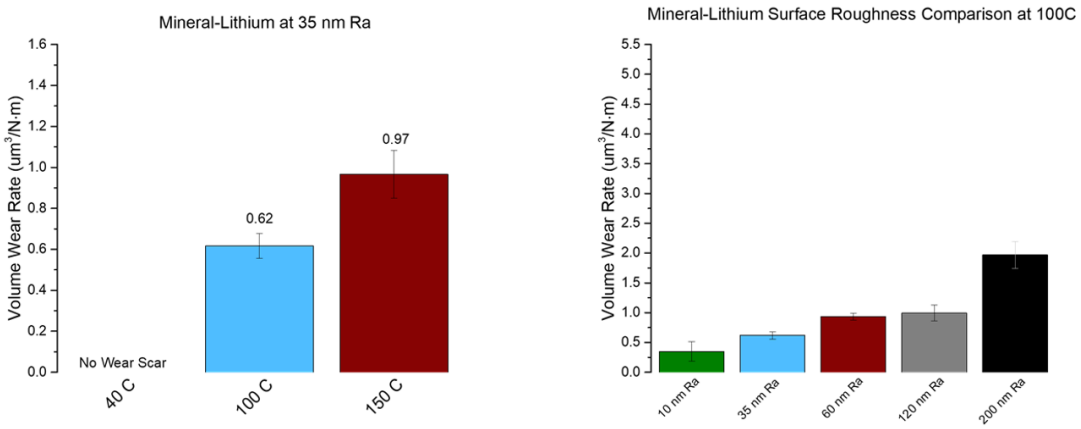

Figure A.4: Mineral-Lithium Grease: Ball on disk volume wear rate averages.

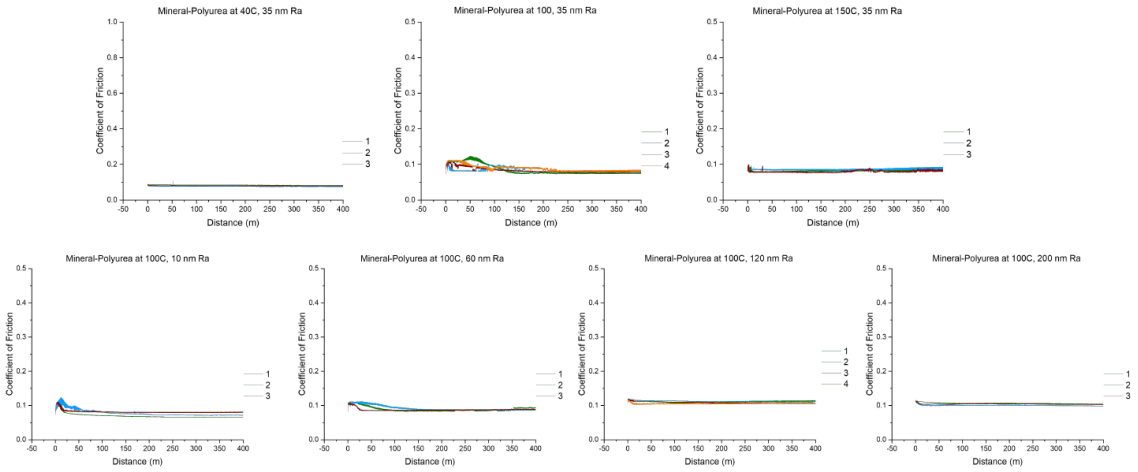

Figure A.5: Mineral-Polyurea Grease: Ball on disk friction behavior for each individual test at each tested temperature.

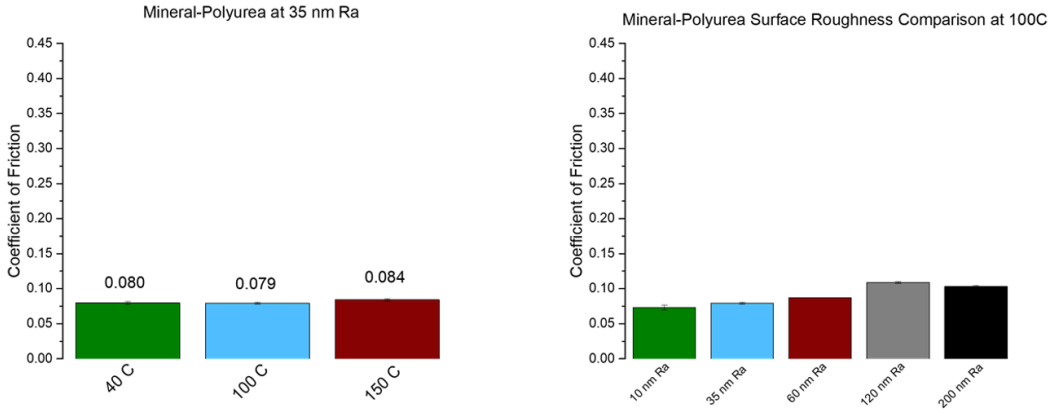

Figure A.6: Mineral-Polyurea Grease: Ball on disk friction averages.

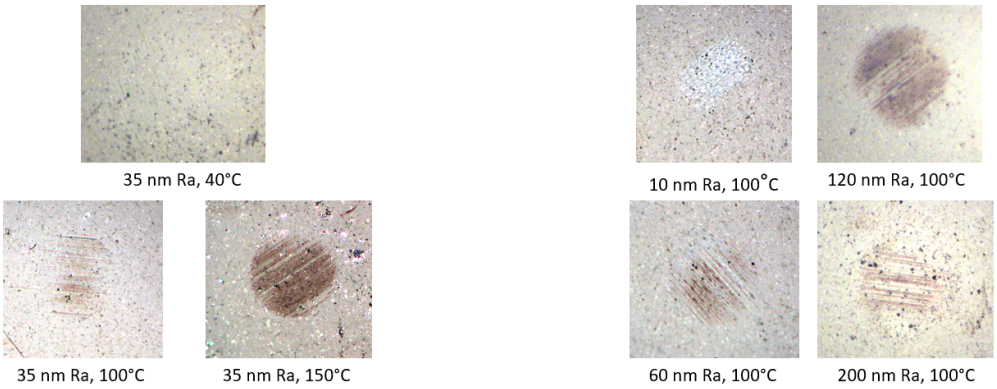

Figure A.7: Mineral-Polyurea Grease: Representative wear scars for each tested condition using the ball on disk test parameters. Images are at 10x.

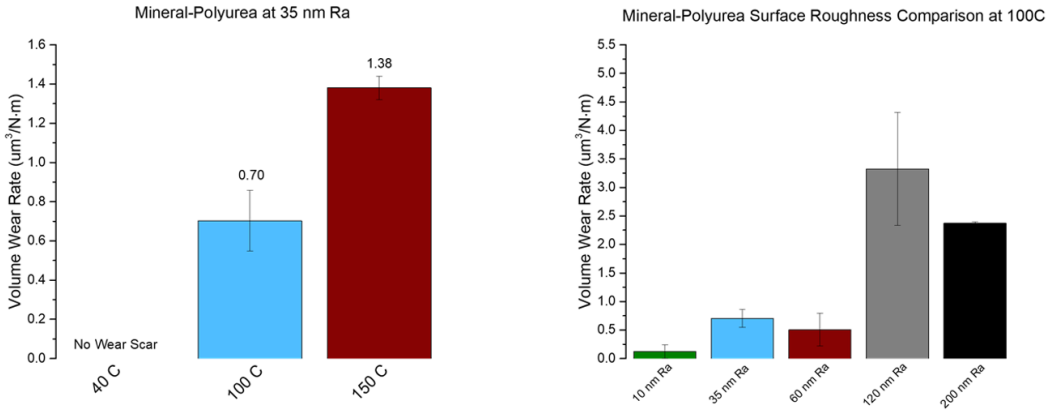

Figure A.8: Mineral-Polyurea Grease: Ball on disk volume wear rate averages.

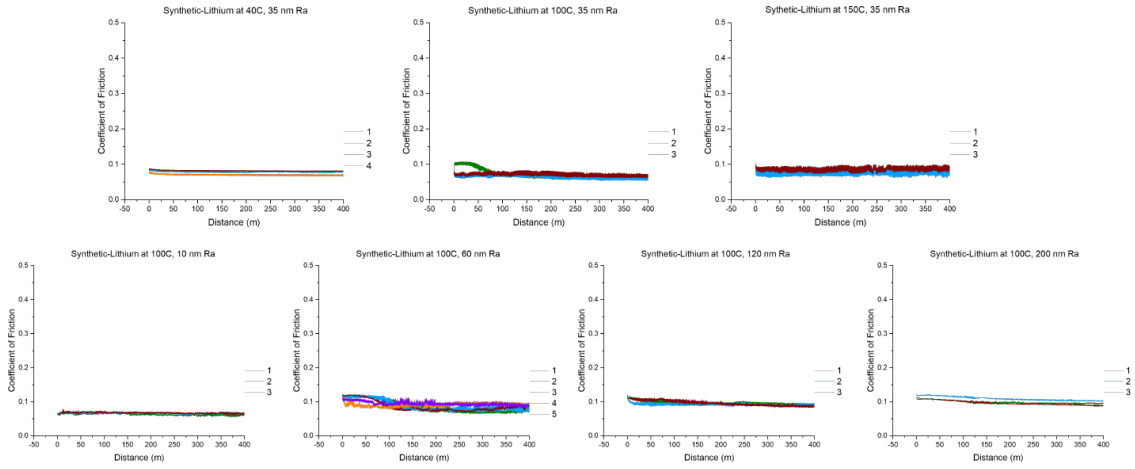

Figure A.9: Synthetic-Lithium Grease: Ball on disk friction behavior for each individual test at each tested temperature.

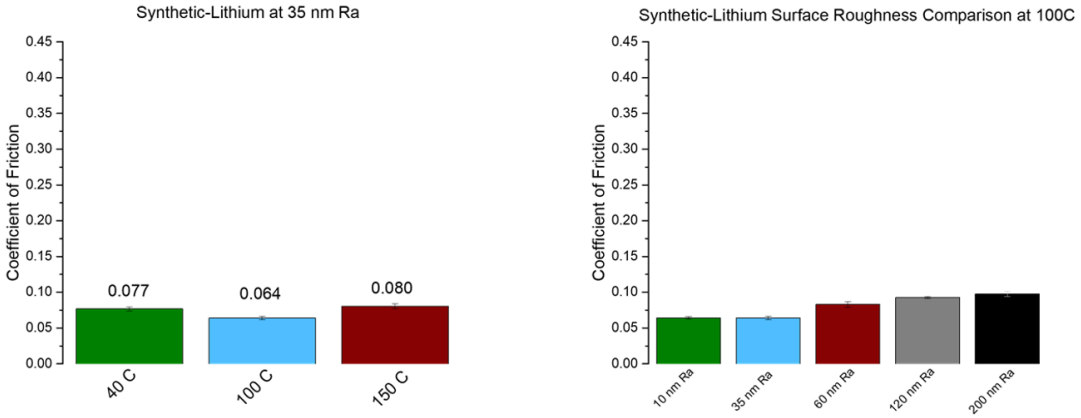

Figure A.10: Synthetic-Lithium Grease: Ball on disk friction averages.

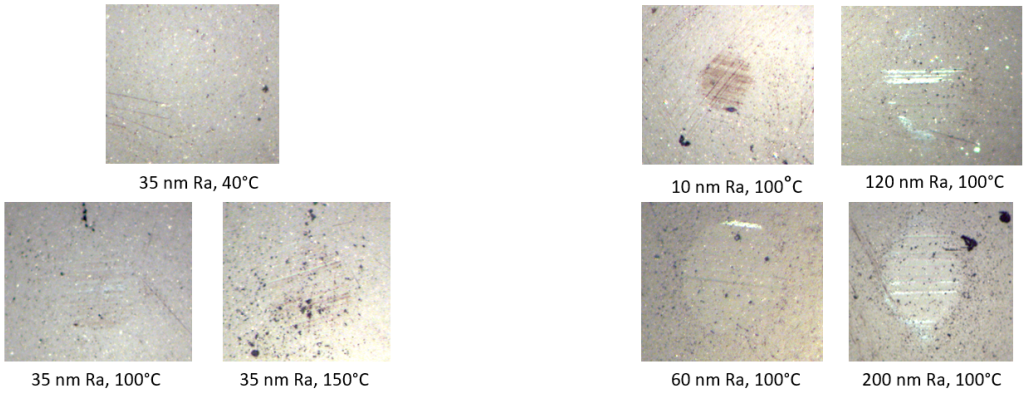

Figure A.11: Synthetic-Lithium Grease: Representative wear scars for each tested condition using the ball on disk test parameters. Images are at 10x.

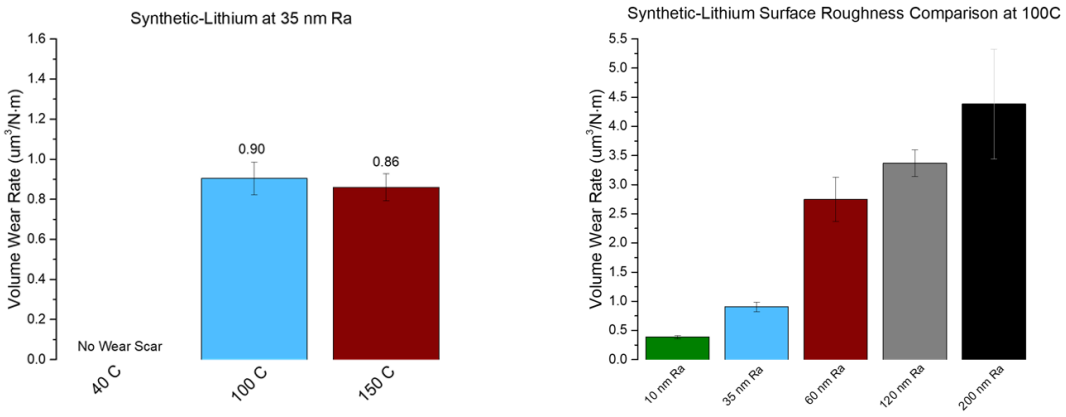

Figure A.12: Synthetic-Lithium Grease: Ball on disk volume wear rate averages.

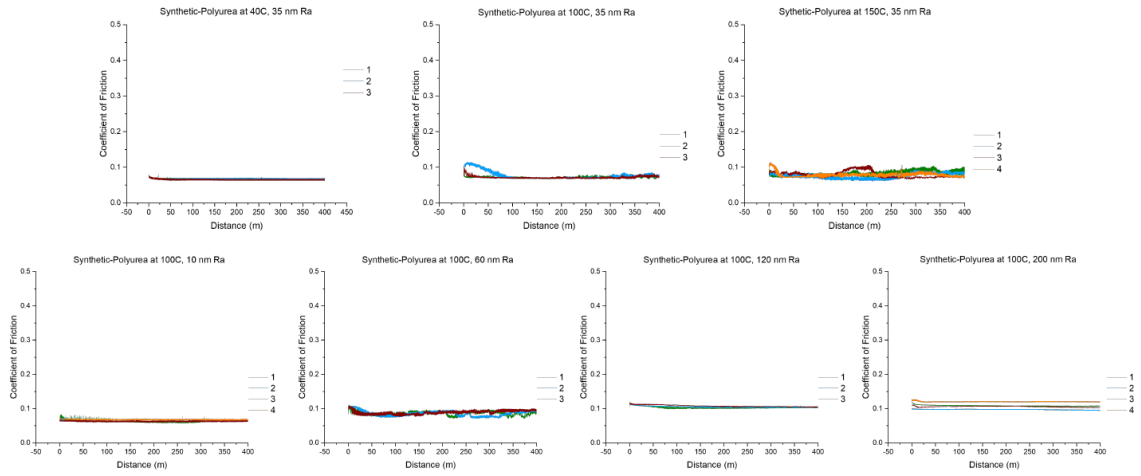

Figure A.13: Synthetic-Polyurea Grease: Ball on disk friction behavior for each individual test at each tested temperature.

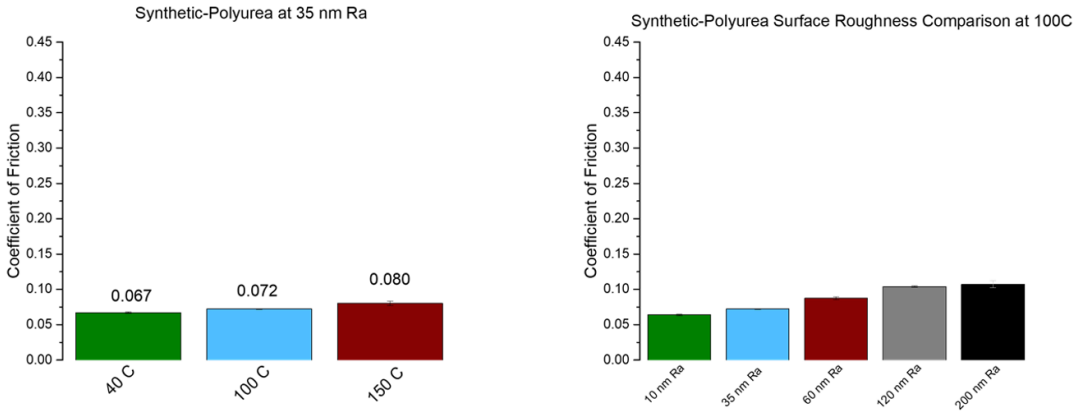

Figure A.14: Synthetic-Polyurea Grease: Ball on disk friction averages.

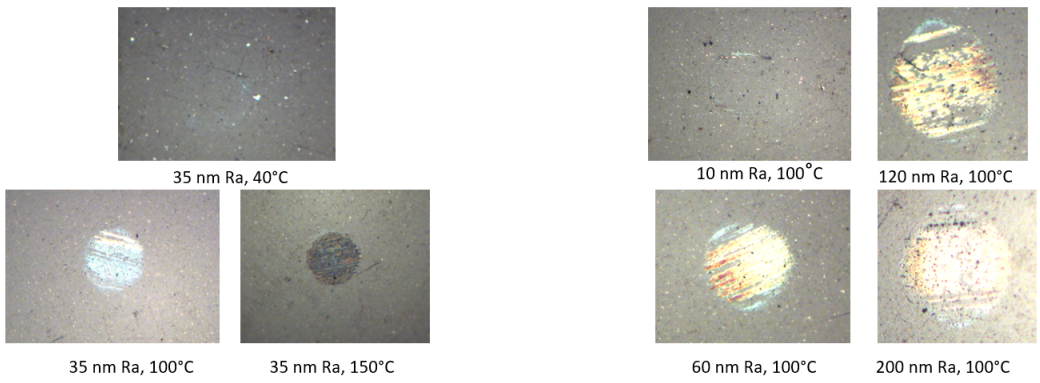

Figure A.15: Synthetic-Polyurea Grease: Representative wear scars for each tested condition using the ball on disk test parameters. Images are at 10x.

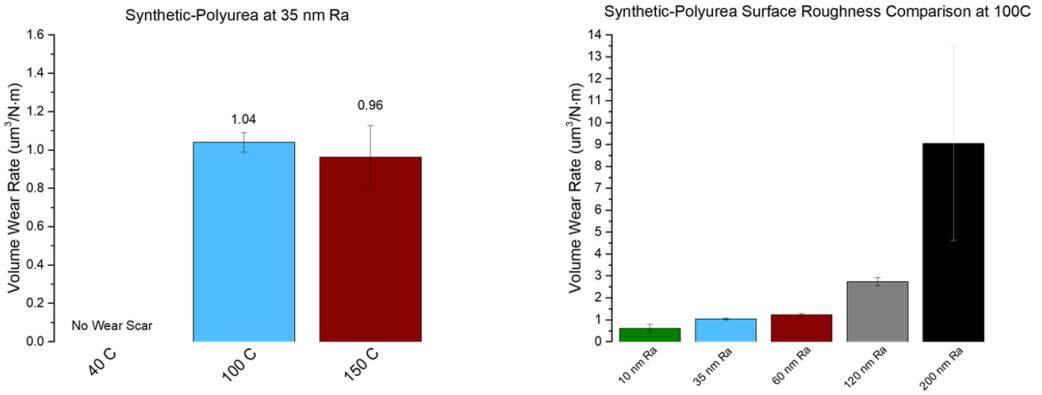

Figure A.16: Synthetic-Polyurea Grease: Ball on disk volume wear rate averages.

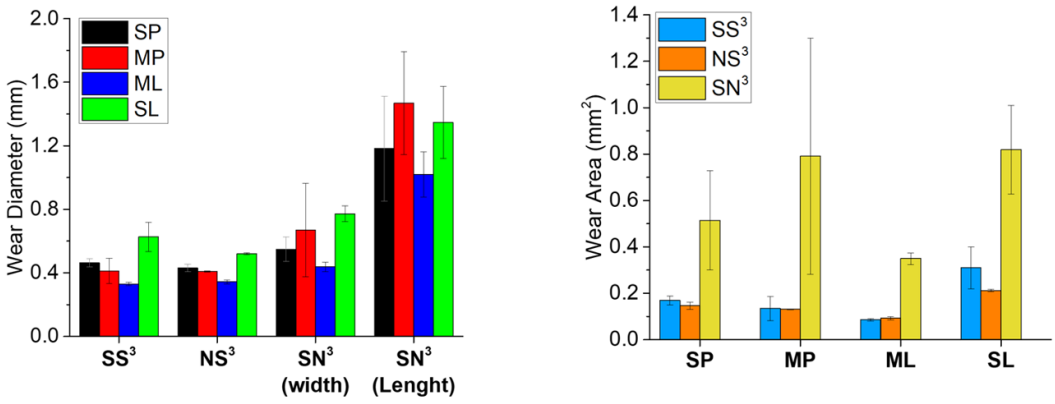

Figure A.17: Four-Ball wear results presented as wear diameter and wear area. Plots provide wear data for each grease and test configuration.

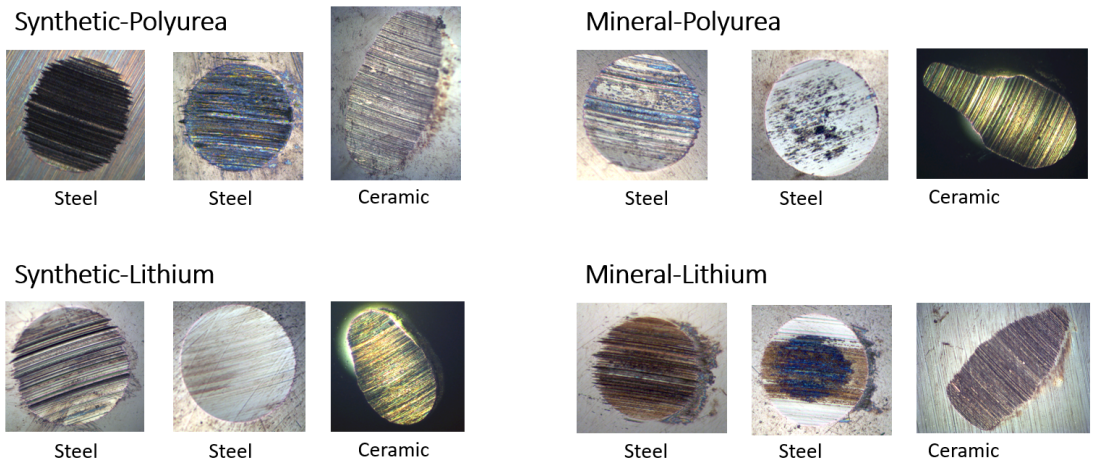

Figure A.18: Representative wear scars for each grease and tested configuration using the four-ball test parameters. Images are at 10x.